Experiments with the dynamics of the Riemann zeta function (preliminary draft)

Barry Brent

9 March 2017

Abstract

We collect experimental evidence for several propositions, including the following: (1) For each Riemann zero ρ (trivial or nontrivial) and each zeta fixed point ψ there is a nearly logarithmic spiral $s_{\rho,\psi}$ with center ψ containing ρ. (2) $s_{\rho,\psi}$ interpolates a subset $B_{\rho,\psi}$ of the backward zeta orbit of ρ comprising a set of zeros of all iterates of zeta. (4) If zeta is viewed as a function on sets, $\zeta(B_{\rho,\psi}) = B_{\rho,\psi} \cup \{0\}$. (5) $B_{\rho,\psi}$ has nearly uniform angular distribution around the center of $s_{\rho,\psi}$. We will make these statements precise.

1   INTRODUCTION

1.1   Overview.

For complex w, let $\zeta^{\circ-}(w)$ denote the backward zeta orbit of w so that $\zeta^{\circ-}(w) = \{s \in \mathbf{C} \text{ s.t. some iterate of zeta takes } s \text{ to } w\}$. If the sequence $B = (a_0, a_1, a_2, ...)$ satisfies $a_0 = w$ and $\zeta(a_n) = a_{n-1}$ for all $n \geq 1$, we say that B is a branch of $\zeta^{\circ-}(w)$. If B converges with $\lim B = \lambda$, say, we conjecture that B is unique and we write B as $B_{w,\lambda}$. We collect numerical evidence supporting the following claims, which will be made precise below: (1) that for each of a countable set of non-real zeta fixed points ψ and each nontrivial Riemann zero ρ, $B_{\rho,\psi}$ exists, is unique, and is the center of a nearly logarithmic spiral, say $s_{\rho,\psi}$, interpolating $B_{\rho,\psi}$; (2) that the members of $B_{\rho,\psi}$ are distributed nearly uniformly on $s_{\rho,\psi}$; (3) and that there is another set of real zeta fixed points $\psi = \psi_{-2n}$ near the trivial zeros $-2n$, $-2n \leq -20$, such that consecutive members of $B_{\rho,\psi_{-2n}}$ rotate around ψ_{-2n} through an angle of $\approx \pi$ or 2π, depending upon the parity of n, so that the members of $B_{\rho,\psi_{-2n}}$ lie on a curve that is very nearly a straight line passing through both ψ_{-2n} and ρ. These claims suggest that (eventually) there may be a statement equivalent to the Riemann hypothesis based on a dictionary relating zeta fixed points to zeta zeros. Some of the claims can be generalized to fixed points of zeta iterates (members of zeta cycles.) We have not proved any theorems. Our experiments were done with *Mathematica* and spot-checked with *Sage*.

1.2 More definitions.

Let ζ denote the Riemann zeta function and let us write the iterates of a function f as $f^{\circ 0}(z) = z$ and $f^{\circ(n+1)}(z) = f(f^{\circ n}(z))$ for $n = 0, 1, \dots$. An n-cycle for f is an n-tuple $(c_0, \dots, c_{n-1})$ such that $f(c_{n-1}) = c_0$ and $f(c_k) = c_{k+1}$ when $k \neq n - 1$. The forward orbit of w under f is the sequence $(w, f(w), f^{\circ 2}(w), \dots)$. The backward orbit of w under f is the set of complex numbers s such that $f^{\circ n}(s) = w$ for some integer $n \geq 0$. Let the symbol $f^{\circ -}(w)$ denote this backward orbit; if w does not belong to a cycle, $f^{\circ -}(w)$ carries the structure of a rooted tree in which the root is w and the children of $s \in f^{\circ -}(w)$ are the solutions t of $f(t) = s$. We will call any path in $f^{\circ -}(w)$ that begins at w a branch of $f^{\circ -}(w)$ (also: "a branch of the inverse of f".) Such a branch, then, is a sequence $(a_0, a_1, a_2, \dots)$ with $a_0 = w$ and $a_n = f(a_{n+1})$ for each non-negative integer n. Since the Riemann hypothesis has been verified within the range of our observations, we write without ambiguity ρ_k for the kth nontrivial Riemann zero ordered by height above the real axis and ρ_{-k} for its complex conjugate. If $\zeta^{\circ n}(z) = 0$ and $\zeta^{\circ n-1}(z)$ is a nontrivial Riemann zero, we call z a nontrivial zero of $\zeta^{\circ n}$. For typographical reasons, we will occasionally write ζ_n for $\zeta^{\circ n}$; within our article, there should no confusion with other common uses of this symbol.

For $z \in \mathbf{C} \cup \{\infty\}$, $A_z := \{u \in \mathbf{C} \text{ s.t. } \lim_{n \to \infty} \zeta^{\circ n}(u) = z\}$ (the "basin of attraction" of z under zeta iteration.) Let $\phi \approx -.295905$ be the largest negative zeta fixed point. Then A_ϕ is a fractal [11]; each nontrivial Riemann zero appears to lie in an irregularly shaped bulb of A_ϕ (Figures 1.1, 3.2, and section 3 more generally.)

For a spiral s with center γ, let α be the point on the intersection of the critical line and s closest to γ. We define a real-valued function $\theta(z)$ on complex numbers $z \in s, |z - \gamma| \leq |\alpha - \gamma|$ by requiring that $\theta(z) \equiv \arg(z - \gamma) \pmod{2\pi}$, and that $\theta(z)$ increases continuously and monotonically as z moves around s from α in the direction of decreasing $|z - \gamma|$. In other words, $\theta(z)$ behaves up to a multiplicative constant like a winding number. If a sequence $(a_1, a_2, \dots)$ lies on a spiral s with center γ and for some pair of real numbers $A > 0, B > 0$ and all $k = 1, 2, \dots, |\theta(a_k) - \theta(a_{k+1})| < Ae^{-Bk}$, we will say that the a_k are distributed nearly uniformly around s.

For complex z, let $r(z) := |z - \gamma|$. Let m, b be real numbers, so that $r(z) = \exp(m\theta(z) + b)$ describes a logarithmic spiral with center γ and typical element $\exp(m\theta(z) + b) \exp(i\theta(z))$. Suppressing the dependence on m and b, let

$$d(\gamma, z) := \left| \frac{z - \gamma - \exp(m\theta(z) + b) \exp(i\theta(z))}{z - \gamma} \right|.$$

We say that s is c-nearly logarithmic for real positive c if

$$\max_{z \in s, 0 < |z - \gamma| \leq |\alpha - \gamma|} d(\gamma, z) < c$$

2

for some m and b.

We require a notion of "very nearly a straight line" to state one of our claims more precisely. Suppose (1) a complex curve C of finite arc length has an initial point z_I and terminates at a point z_T, (2) that there are real numbers m and b such that

$$\lim_{z \in C, z \to z_T} \left| \frac{\Im(z) - (m\Re(z) + b)}{\Im(z)} \right| = 0,$$

and (3) that the convergence has exponential decay as $|z - z_T|$ decreases from $|z_I - z_T|$ to zero. Then we say that C is very nearly a straight line.
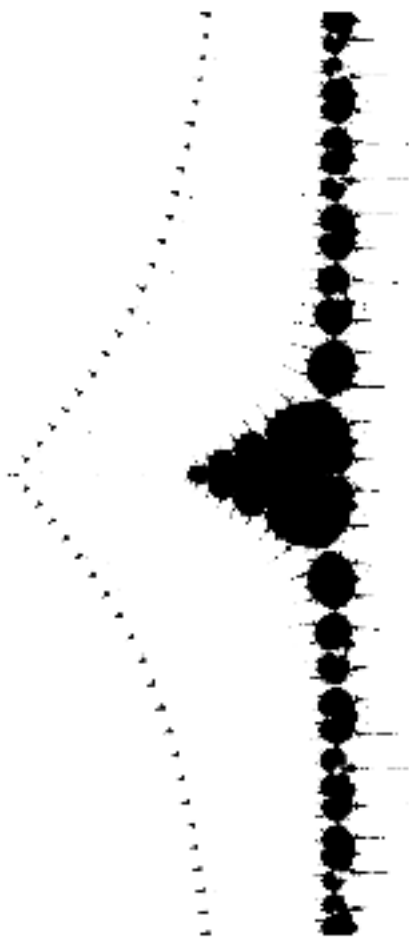

FIG. 1.1: A_ϕ

1.3 Summary of observations.

We express some of our observations as explicit conjectures.

Conjecture 1 *For each pair of positive integers L and n, there is a Riemann zeta L-cycle Λ such that the $\lambda \in \Lambda$ with maximum imaginary part is close to the nth nontrivial zero ρ_n (but we will not define this use of the term "close" more precisely in this draft) and with the following properties.*

(1) Each $\lambda \in \Lambda$ is a repelling fixed point of $\zeta^{\circ L}$ lying in the intersection of boundaries $\partial A_\phi \cap \partial A_\infty$ in the usual topology on $\mathbf{C}$.

(2) For each $\lambda \in \Lambda$ there is a complex number z_λ and a natural number $0 \leq j_\lambda \leq L - 1$ such that
(a) $\zeta^{\circ j_\lambda}(z_\lambda) = \rho_n$.
(b) For some small positive c, λ is the center of a c-nearly logarithmic spiral $s_{z_\lambda, \lambda}$ interpolating a branch $B_{z_\lambda, \lambda}$ of $(\zeta^{\circ L})^{\circ -}(z_\lambda)$ (but we will not be more precise about this use of the term "small" in this draft.)
(c) If $L = 1$, so that the unique element of Λ is close to ρ_n, then we write $\Lambda = \{\psi_n\}$, and we have that $j_{\psi_n} = 0$ and $z_{\psi_n} = \rho_n$. In this situation, we can take $c < e^{-4}$; furthermore, if $L = 1$, then the infimum of the valid values of c in clause (b) goes to zero as $n \to \infty$.
(d) $\lim B_{z_\lambda, \lambda} = \lambda$.
(e) $\bigcup_{\lambda \in \Lambda} B_{z_\lambda, \lambda}$ is a branch $B_{\rho_n, \Lambda}$ of $\zeta^{\circ -}(\rho_n)$.
(f) The members of $B_{z_\lambda, \lambda}$ are distributed nearly uniformly on $s_{z_\lambda, \lambda}$.

(3) If $z \in \zeta^{\circ -}(\rho_n)$ then for some positive integer j and some positive integer L and some L-cycle $\Lambda, \zeta^{\circ j}(z) \in B_{\rho_n, \Lambda}$.

Some evidence for this conjecture appears in section 6.1.1.

When $L = 1$ we have restricted our claims in this conjecture to spirals s_{ρ_n, ψ_n} because that is the case we have checked most thoroughly, but we have also checked less thoroughly the case in which the zero is fixed (usually, ρ_1) and ψ_n varies over positive n. It appears to us that the conjecture generalizes to all pairs $\rho = \rho_{n_1}, \psi = \psi_{n_2}, (n_1, n_2) \in \mathbf{Z}^{\geq 1} \times \mathbf{Z}^{\geq 1}$.

Because $\lambda \in \Lambda$ would be repelling, it would also be an attracting fixed point of a local branch of the functional inverse of $\zeta^{\circ L}$, and then the convergence would follow from standard results, for example, Theorem 2.6 of [4].

Conjecture 2 *(1) There are repelling zeta fixed points ψ_{-2n} near the trivial zeros $-2n \leq -20$.*
(2) For any nontrivial Riemann zero ρ, members of $B_{\rho, \psi_{-2n}}$ lie on a curve which is very nearly a straight line segment. If n is even, the endpoints are ρ and ψ_{-2n}; otherwise, the curve passes through ψ_{-2n} and terminates at ρ.

(3) If $2n \equiv 0$ (mod 4), then

$$\arg \frac{d\zeta(\psi_{2n})}{dz} \approx 2\pi;$$

If $2n \equiv 2$ (mod 4), then

$$\arg \frac{d\zeta(\psi_{2n})}{dz} \approx \pi.$$

(See Figure 5.7. Some evidence for this conjecture appears in section 6.1.2.) These observations are consistent, of course, with the proposition that $B_{\rho,\psi_{-2n}}$ is interpolated by a spiral. Our computations of $\zeta(x) - x$, x real, indicate that the ψ_{-2n} are real (the graph crosses the x-axis near each trivial zero we examined.) It was conceivable that there might be a broader relationship of the same kind between the derivative of zeta at a given fixed point and the structure of the associated spirals centered at those fixed points elsewhere in the complex plane, but our experiments have not verified any such relationship. It is suggestive, of course, that these relationships are exact when zeta is considered as a function of real numbers and ψ_{-2n} is replaced by $-2n$.

We examined the possibility that branches of $\zeta^{\circ-}(z), \zeta(z) \neq 0$ for arbitrary z on the critical line converge to the same fixed points as branches of $\zeta^{\circ-}(\rho), \rho$ a non-trivial zero. We tested various such z and found spiral branches converging to the fixed points of zeta. So it ought be possible to explain the spirals with a theory that avoids any appeal to special properties of the Riemann zeros. We are not going to describe these experiments in any further detail in this article.

An analogy from fluid mechanics led us to check for invariance of branches of $\zeta^{\circ-}(z)$ for these z under rotation about the fixed points at their centers. We found that the deviation from this sort of invariance is systematic and can itself be described by referring to (other) logarithmic spirals.

We made a brief survey of functions other than zeta to gauge the extent of the spiral phenomenon, which we will not describe in any further detail than the following. Functions as simple as cosine appear to exhibit this behavior. We also observed it in, for example, the Ramanujan L-function. We hope to carry out another survey with a different software package.

1.4   Prior work.

Many authors have examined the Riemann zeta function with computers. Notable citations from the perspective of this article are Arias-de-Reyna [3], Broughan [1], Cloitre, [2], Kawahira [5], King [6, 7] and Woon [11].

2 METHODS

2.1 Quadrant plots.

We will be displaying colored plots (say, "quadrant plots") depicting, for a point w of $\mathbf{C}$ and a meromorphic function f, the quadrant of $f(w)$. We use quadrant plots in three ways: (1) to determine small squares containing exactly one solution of an equation of interest, so that this information can be used by standard equation-solving routines to find a solution to several hundred digits of precision (which we find is necessary, for example, to locate zeta cycles) lying in a particular region; (2) to superimpose quadrant plots upon plots of the basin of attraction A_ϕ. These two kinds of plot typically interlock in a way that helps us to understand the meaning of many small irregular features of A_ϕ; and (3) to show how the quadrant plots spiral as we reduce the size of the plot window about a fixed point of zeta or one of its iterates. Observation of these spiral motions was our first indication that forward orbits near fixed points do lie on spirals.

In quadrant plots, the boundaries of single-colored regions are f pre-images of the axes–curves corresponding to zero sets of $\Re(f(s))$ and $\Im(f(s))$; the apparent intersections signal the presence of zeros or poles of f. By adjusting the color scheme to distinguish between regions where $|f|$ is large or small, we can try to distinguish zeros from poles. Some apparent intersections are revealed to be illusions by a change of scale. Similar but colorless methods for plotting zeros were put to use in [3].

The visualized region is partitioned into small squares, each of which is represented by a pixel. We choose a test point s in each square. The pixel representing the square is colored according to the rules in Table 1. In the table, the region D is a disk with center $s = 0$ and large radius r (chosen as may be convenient.) We denote the complement of D as $-D$.

Location of $f(s)$	Color of pixel depicting region containing s
real and imaginary axes	black
$D \cap$ Quadrant I	rich blue
$-D \cap$ Quadrant I	pale blue
$D \cap$ Quadrant II	rich red
$-D \cap$ Quadrant II	pale red
$D \cap$ Quadrant III	rich yellow
$-D \cap$ Quadrant III	pale yellow
$D \cap$ Quadrant IV	rich green
$-D \cap$ Quadrant IV	pale green

TABLE 1: COLORING SCHEME FOR QUADRANT PLOTS

The junction of four rich colors represents a zero, the junction of four pale colors represents a pole, and the boundary of two appropriately-colored regions is an

f pre-image of an axis. An example is shown in Figure 2.1: $s \mapsto (s-1)^2(s-i)(s+1)^5/(s+i)^3$. (We have superimposed a pair of axes on this quadrant plot.)
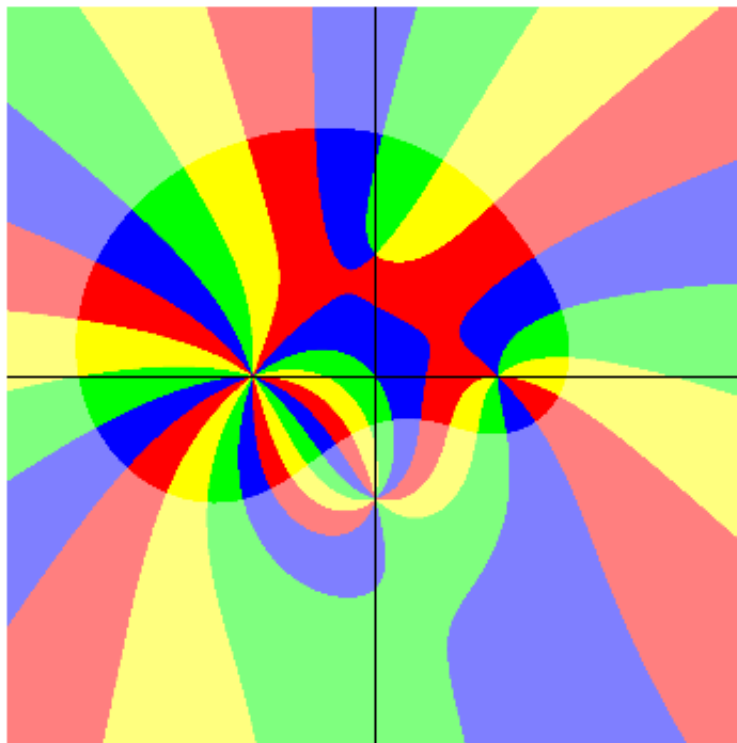

FIG. 2.1: QUADRANT PLOT OF $s \mapsto (s-1)^2(s-i)(s+1)^5/(s+i)^3$

2.2 High precision equation solving under geometric constraints.

FIG. 2.2: ZOOMING IN ON λ_1 VIA QUADRANT PLOTS OF $\zeta^{\circ 3}(s) - s$

We illustrate the application of quadrant plots to solve equations under geometric constraints by showing how we found the three-cycle Λ described in section 5.4. In Figure 2.2, we have superimposed plots of A_ϕ and quadrant plots of $s \mapsto \zeta^{\circ 3}(s) - s$ on small squares near the first non-trivial Riemann zero. The resolution has been kept low to speed up the computations; high resolution is not particularly helpful in this situation. The left panel is a square with side length 20 and center ρ_1. The central panel depicts a square with side length 2 and center $\rho_1 + 3.4 + .1i$; we have adjusted the center to keep in view a particular four-color junction visible in the left panel. It represents a solution of $\zeta^{\circ 3}(s) - s = 0$, namely the three-cycle element λ_1 we are trying to compute. At this stage, if we used, for example, the *Mathematica* command FindRoot constrained to search within this square, it might land on any one of the several four-color junctions we see in the central panel. So we change the center of the plot again, this time to $\rho_1 + 3.46 + .103i$, and we make a square plot centered there with side length .02. This is shown in the right panel of Figure 2.2. Next we use a slow, "handmade" routine to approximate λ_1 by searching within this square. Then, using this approximation as the beginning value for a search with FindRoot, we obtain a solution with 500 digits of precision:

3.958962334884743467351645843989612346147703995186680145588250655505433123571979761912916043252683212642851541785632624240842212449077589537219976674458409141742662175701089081252727395073714398968532356378122551383020846341495246708099651447035416573604285022308201354286093853689445394424111643849274624319987800123899354077015803481697894786604286381153651800267403339424674272845152302295507932862394783352056753229824400444229415683734237098200233087407432207677718574620773032348240609461428004 6

+14.236228563221813322871223010855881692998712362084943995686954378256069322896396761526007136189745757467102551375667154010366364994538731791627111382325375111094897277576221794166383077071426204175566403532396710787895292044043947643155315825880513523093272920043436541351728 20

77800178612380069991096443831984716653028230153558652029712771878476691974168218415293165267046606327405458655765280027732495125802150527924572824108341915071076583938484583136641136239358002932626787007916001254650107668 53i.

Let us denote this approximation of λ_1 as a. A numerical check indicates that $|\zeta^{\circ 3}(a) - a|$ agrees with zero to 495 decimal places.

Our main reason for requiring so much precision is that we will be repeatedly solving equations of the form $\zeta(u) = v$ for u, in each case replacing v with the previous u, to construct lists of (usually) 100 elements of a branch of the backward orbit of a nontrivial Riemann zero, looking for the u's near pre-selected fixed points. As the procedure repeats 100 times, there is an accumulation of numerical error, and in this situation very high precision is needed to maintain enough accuracy to "see" the spirals formed by these branches in our plots.

3   A TOUR OF A_ϕ

We are interested in A_ϕ because plots of this set make visible the underlying structure of the network of $\zeta^{\circ n}$ pre-images of the critical line for all n at once: (1) the nontrivial zeros of the $\zeta^{\circ n}$ lie in bulbs of A_ϕ on filaments F decorating the border of A_ϕ, and (2) one $\zeta^{\circ n_F}$ pre-image of the critical line transects each such F. (Claims 1 and 2 are not, of course logically equivalent; we are summarizing computer observations that we will describe in more detail below.) Thus the structure of union of rooted trees visible in plots of A_ϕ is apparently graph-isomorphic to a corresponding structure for the point set

$$\bigcup_{\Re(z)=\frac{1}{2}} \zeta^{\circ -}(z) = \mathcal{U} \text{ (say.)}$$

This observation informs our discussion of the trees T in the next section. We pretend that we have stated a rigorous definition of the decoration notion and definite conditions for the membership of a given complex number in a given filament. In view of the relationship between $\mathcal{U}$ and A_ϕ, this should not cause problems: each filament F may be identified with one (of the many) $\zeta^{\circ n_F}$ pre-images of the critical line, the definition of which could be made precise. But we should say explicitly that "A decorates B" is a transitive relation and that the filaments are subsets of A_ϕ.

In Figure 3.1, for example, the points at the junctions of four colors represent zeros of $\zeta^{\circ 2}$; the zeros in the long filaments are nontrivial. The right panel of Figure 3.2 shows a quadrant plot of $s \mapsto \zeta(s) - s$ superimposed on a plot of A_ϕ; the fixed points of zeta appear as the junction of four colors. The left panel depicts the nontrivial Riemann zeros using the same scheme (a quadrant plot of zeta.)
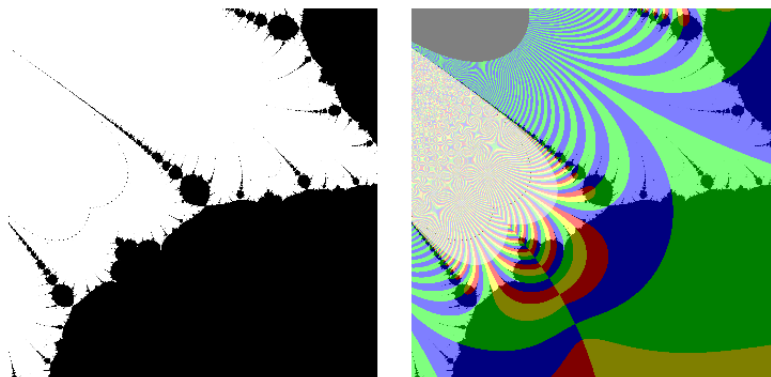
9

FIG. 3.1: LEFT: A_ϕ AT THE EDGE OF THE MAIN CARDIOID; RIGHT: SUPERIMPOSED QUADRANT PLOT OF $\zeta^{\circ 2}$
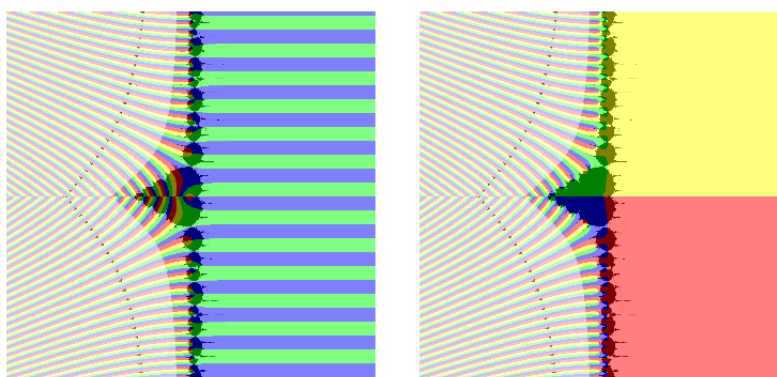

FIG. 3.2: LEFT: QUADRANT PLOT OF ZETA; RIGHT: QUADRANT PLOT OF $\zeta(s) - s$; BOTH SUPERIMPOSED ON A_ϕ

10

The filled Julia set of zeta (the points in $\mathbf{C}$ with bounded orbit under iteration by zeta) is $\mathbf{C} - A_\infty$. The basin A_ϕ appears to be dense in $\mathbf{C}$ - A_∞. The sets $\mathbf{C}$ - A_∞ (Figure 3.3) and A_ϕ, regarded as regions in the complex plane, are indistinguishable in our plots but they are not identical. For example, there is
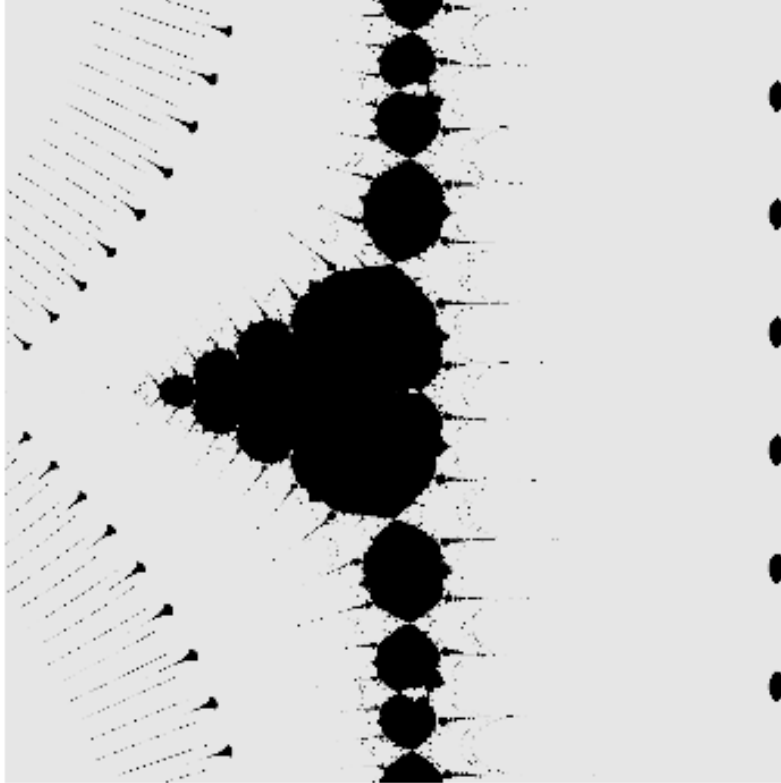
FIG. 3.3: $\mathbf{C}$ - A_∞

an infinite number of real zeta fixed points ([11], Theorem 1) that belong to $(\mathbf{C} - A_\infty) - A_\phi$. In addition, there appear to be infinite families of non-real zeta k-cycles for each integer $k \geq 1$ in $(\mathbf{C} - A_\infty) - A_\phi$.

Zero lies in A_ϕ ([11], Theorem 1.) This set is a fractal decorated with numerous long filaments (Figure 3.1.) Zeroes of the $\zeta^{\circ n}$ lie on the filaments. Because zero is an element of A_ϕ, we know that the whole backward orbit $\zeta^{\circ -}(0)$ lies in A_ϕ. Because the pre-images of nontrivial Riemann zeros under iterates of zeta lie on the filaments, the itinerary of a point in the backward orbit of a nontrivial zero ρ visits several filaments at the edge of A_ϕ before coming to ρ. (Some but not all pre-images of the trivial zeros also lie on filaments.)

11

The set A_ϕ seems to comprise

(1) a heart-shaped, seven-lobed central body, which we will call the main cardioid.

(2) two major filaments of bulbs of various irregular shapes that emanate from the main cardioid, transected by the critical line and containing one nontrivial Riemann zero in each bulb (right panel of Figure 3.2.)

(3) infinitely many blunt processes and long filaments decorating the main cardioid and each of the irregular bulbs. The filaments comprise smaller copies of the bulbs, which, in turn, are decorated with similar filaments, *ad infinitum*. (Figure 3.1.) Thus, when we plot them, the set of filaments decorating A_ϕ exhibit a visible tree structure.

The visible features described in (1) - (3) were evident in Woon's plots of **C** $-A_\infty$ [11]. The filaments appear to be zeta-iterate pre-images (close copies) of the two major filaments. Pre-images of the real axis pass through the blunt processes and contain pre-images of the trivial zeros. For example, the right panel of Figure 3.1, superimposes a quadrant plot of $\zeta^{\circ 2}$ on the left panel, so that junctions of four differently-colored regions each represent a zero of $\zeta^{\circ 2}$. There are three long filaments depicted in this image containing zeros, the immediate zeta images of which are nontrivial Riemann zeros; but between the lower two such filaments is a blunt process transected by a zeta pre-image of the real axis, and we can see another series of $\zeta^{\circ 2}$-zeros lying along this curve. These are zeta pre-images of the negative even numbers.

(4) at each trivial zero < -18, a microscopic, more or less distorted copy (zeta-iterate pre-image) of the entire assemblage described in (1) - (3). (By "microscopic" features we mean features so small that they can only be visualized by a change of scale from that of Figure 3.3.) In Figure 3.4, we show copies of the main cardioid near the trivial zeros $-28, -26, -24, -22$ superimposed on quadrant plots of $\zeta^{\circ 2}$ in the same squares. The size of these features decays exponentially with distance from zero. Their left-right orientation alternates. We speculate that the alternation can be derived from the alternating sign of the real derivative $\frac{d\,\zeta(x)}{dx}|_{x=-2n}$.

Because these copies exist on the left half of the real axis, its zeta pre-images also contain complete copies of A_ϕ. The upper left panel of Figure 3.5 depicts the first bulb in the major filament in the upper half plane. It is a 10 by 10 square centered at ρ_1. Along its border we see an apparently infinite set of filaments alternating with an apparently infinite set of blunt processes. Our tests demonstrate that the filaments are transected by $\zeta^{\circ n}$ pre-images of the critical line for $(n = 1, 2, 3, ...)$, and that the blunt processes are transected similarly by
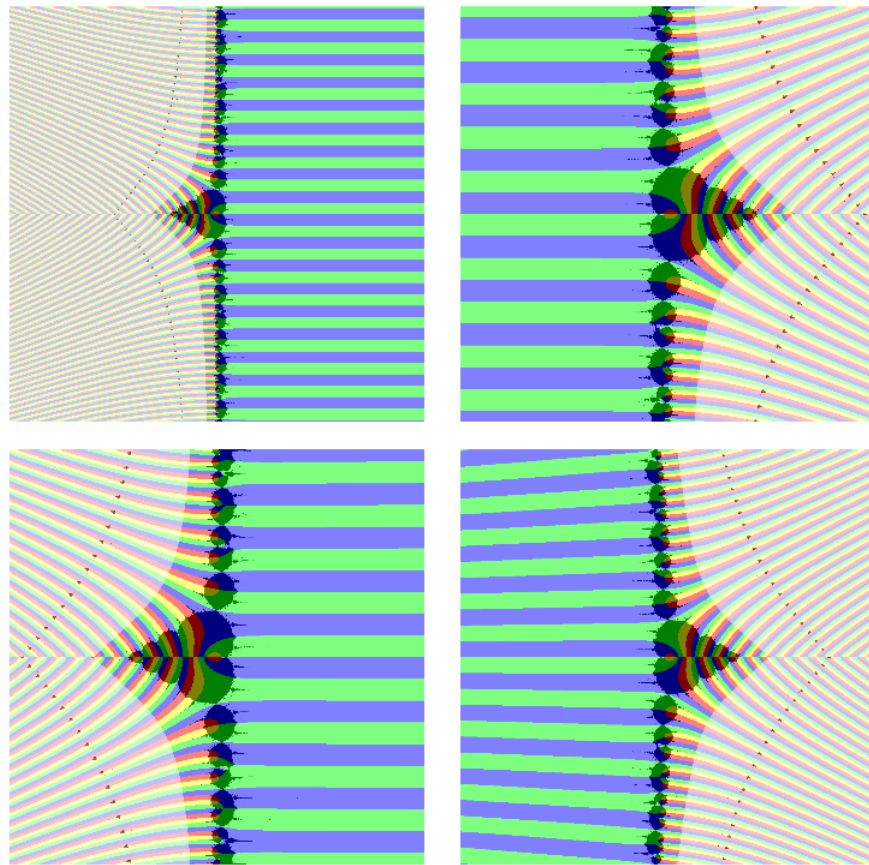
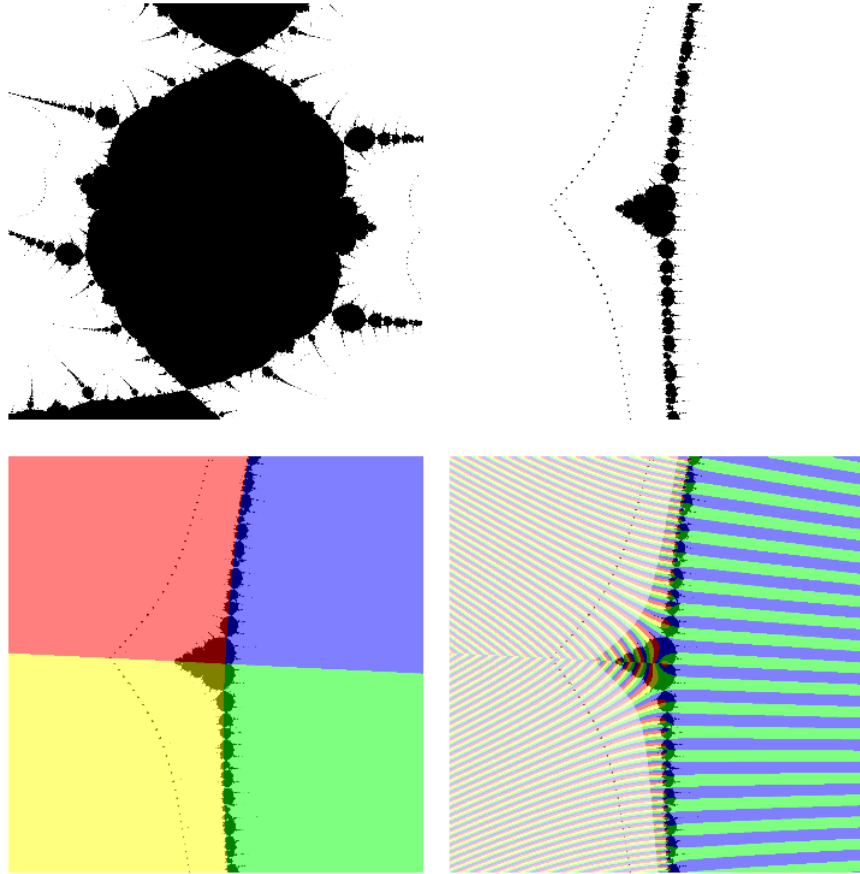FIG. 3.4: A_ϕ COPIES NEAR $s = -28, -26, -24, -22$ SUPERIMPOSED ON $\zeta^{\circ 2}$ QUADRANT PLOTS

13

FIG. 3.5: A COPY OF A_ϕ NEAR A BLUNT PROCESS OF A_ϕ;
LEFT: WITH SUPERIMPOSED QUADRANT PLOT OF $\zeta^{\circ 3}$; RIGHT: SUPERIMPOSED
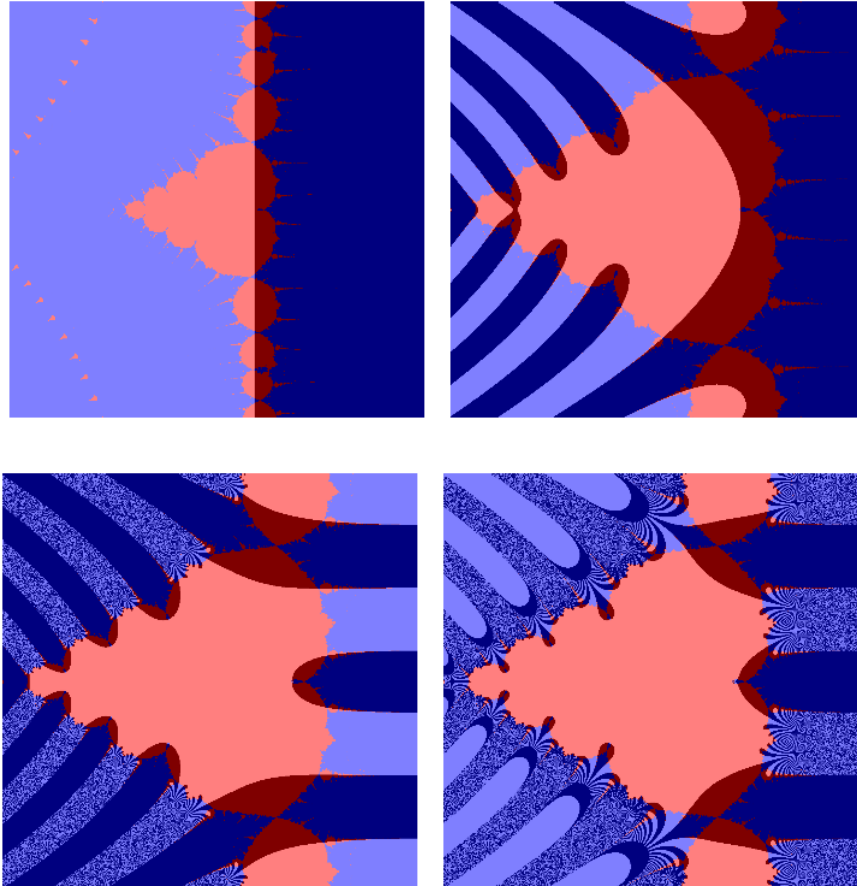QUADRANT PLOT OF $\zeta^{\circ 4}$

FIG. 3.6: DARKER REGIONS ARE $\zeta^{\circ n}$ PRE-IMAGES OF $\Re(s) > \frac{1}{2}$ NEAR THE MAIN CARDIOID; $n = 1$ IN ROW 1 COLUMN 1; $n = 2$ IN ROW 1 COLUMN 2; $n = 3$ IN ROW 2 COLUMN 1; $n = 4$ IN ROW 2 COLUMN 2

$\zeta^{\circ n}$ pre-images of the real axis. The other three panels depict a small copy of A_ϕ to the right of the largest blunt process on the right side of the bulb shown in the upper left panel. In the lower panels, a quadrant plot of $\zeta^{\circ 3}$ in the left panel and of $\zeta^{\circ 4}$ in the right panel have been superimposed upon this copy. Evidently, it is a $\zeta^{\circ 3}$ pre-image of A_ϕ.

(5) Our observations indicate that for each filament F decorating A_ϕ there is a positive integer k_F (say, the degree of F) such that each bulb of F contains one nontrivial $\zeta^{\circ k_F}$ zero, and no nontrivial zeros of $\zeta^{\circ k}$ for any $k \neq k_F$. Even under the Riemann hypothesis, it would not be necessary from first principles that degree k filaments are transected by $\zeta^{\circ k-1}$ pre-images of the critical line, even though that is the simplest possibility. But it seems to be the case. In Figure 3.6, the $\zeta^{\circ k-1}$ pre-images of the critical line transecting degree k filaments decorating the main cardioid are shown for $k = 1, 2, 3$ and 4.

4   BRANCHES INTERPOLATED BY SPIRALS

For any integer $L > 0$ there appears to be an infinite set of zeta cycles $\Lambda = (\lambda_0, ..., \lambda_{L-1})$ that pick out a linearly ordered subset $B_{\rho,\Lambda} = (a_0, a_1, a_2, ...)$ of $\zeta^{\circ -}(\rho)$ such that (1) $a_0 = \rho$, (2) $a_n = \zeta(a_{n+1}), n = 0, 1, 2, ...$ and (3) for each $j = 0, 1, 2, ..., L - 1$, the subsequences $b_j = (a_j, a_{j+L}, a_{j+2L}, ...)$ appear to converge to λ_j. The sequence b_j is a branch of $\zeta_L^{\circ -}(a_j)$. In most of the cases that we have examined, each b_j appears to be interpolated by a spiral s_{ρ_N, λ_j} with center $\lambda_j = \lim b_j$. The λ_j are repelling fixed points of ζ_L.

Now we offer (speaking loosely) a geometric description of some of the b_j in terms of the basin of attraction A_ϕ. (It applies to most, but not all, instances we have examined to date.) A variety of filaments decorate A_ϕ, but here we restrict attention to those that decorate the main cardioid. We assign the set of filaments a structure of union of rooted trees T as follows. A filament $F \in T$ is the parent of a filament $G \in T$ if and only if G decorates F and there is no intermediate filament $H \in T$ such that G decorates H and H decorates F. The filaments containing nontrivial Riemann zeros have no ancestors, but they are not unique in this respect.

Now fix integers $L \geq 1, N \neq 0$. There is an infinite set of zeta L-cycles $\Lambda = (\lambda_0, \lambda_2, ..., \lambda_{L-1})$ such that for each integer $\Delta = 0, 1, 2, ..., L - 1$, there is a tree T_Δ of filaments decorating the main cardioid of A_ϕ, and a path $P_\Delta = (F_0, F_1, ...)$ in T_Δ with $k_{F_m} = \Delta + mL$ and such that (if $m > 0$) F_m decorates the $|N|^{\text{th}}$ bulb of its parent F_{m-1}. As in the first column of Figure 4.1, the filaments in P_Δ spiral around λ_Δ. In our graphic visualizations, the apparent size of F_m decays exponentially with m. Something like this would seem to be a necessary condition of the relation $\lambda_j = \lim b_j$ we mentioned above.

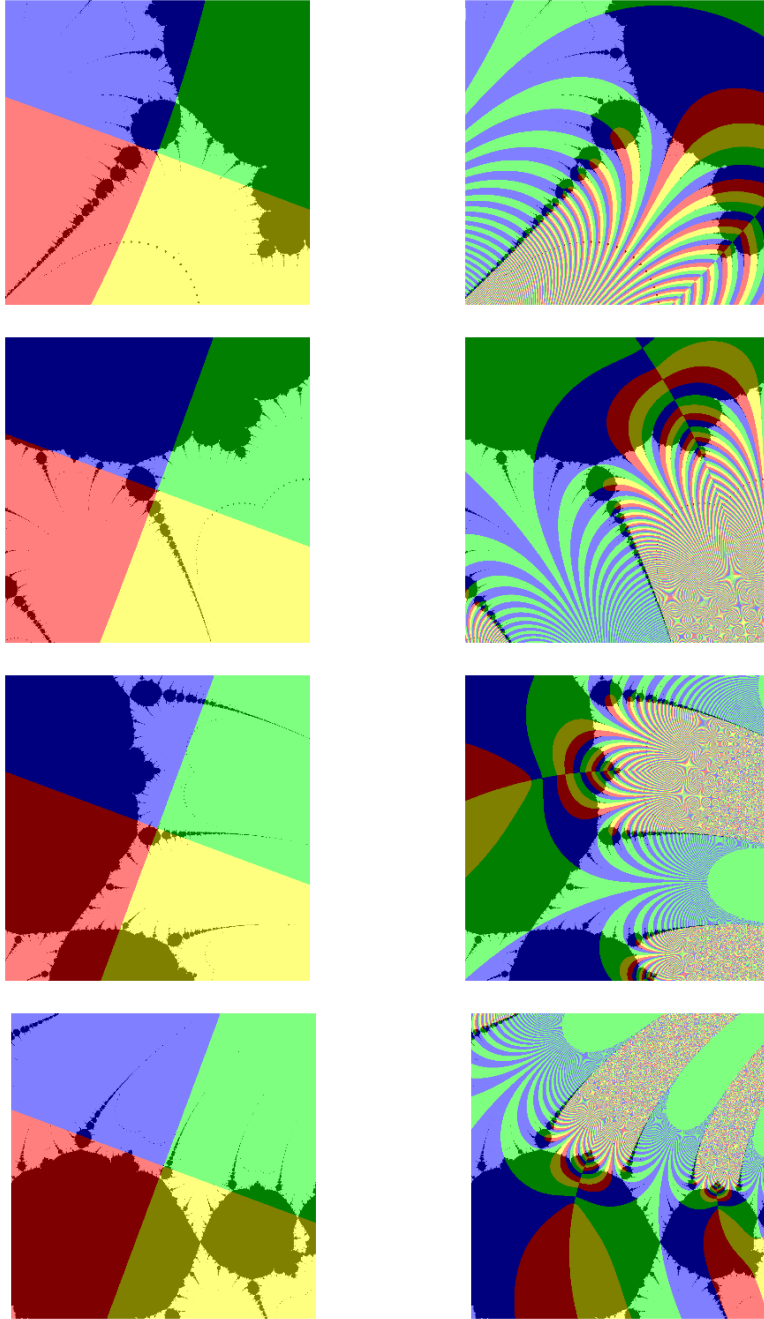Each bulb of F_m contains a nontrivial zero w of $\zeta^{\circ \Delta+mL}$ and $\zeta^{\circ \Delta+mL-1}(w)$

FIG. 4.1: ZOOMING IN ON ψ_{ρ_1}; COLUMN 1: QUADRANT PLOTS OF $\zeta(s) - s$; COLUMN 2 (TOP TO BOTTOM): QUADRANT PLOTS OF $\zeta^{\circ n}, n = 3, 4, 5, 6$

17

is a nontrivial Riemann zero. Which one? Let $w_{m,N}$ be the nontrivial $\zeta^{\circ\Delta+mL}$ zero belonging to the $|N|^{\text{th}}$ bulb of the filament F_m in P_Δ. For $m > 0$, $\zeta_L(w_{m,N}) = w_{m-1,N}$, so the sequence $(w_{0,N}, w_{1,N}, ...)$ is a branch of $\zeta_L^{\circ-}(w_{0,N})$. In our observations, the zeta image of bulb $|N|$ of a filament F in T_Δ with $k_F > 1$ is bulb $|N|$ of its parent filament in T_Δ. Therefore $\zeta^{\circ\Delta+mL-1}(w_{m,N}) = \rho_{\pm N}$.

The observation that $\zeta_L(w_{m,N}) = w_{m-1,N}$ is our evidence for an idea mentioned in the introduction, namely, that there should graph isomorphisms between subgraphs of the rooted tree graphs associated to the $\zeta_L^{\circ-}$ on one side and subgraphs of the trees T decorating the main cardioid of A_ϕ on the other. We should mention that the situation for *copies* of the main cardioid such as the ones illustrated in Figures 3.4 and 3.5 is different; except to say that the zeta images of copies are also copies, we will not discuss it further in the present article.

5   SPIRALS INTERPOLATING A BRANCH OF $\zeta^{\circ-}(\rho)$

5.1   Single spirals interpolating a branch.

When $L = 1$, $\Lambda = \{\lambda_1\}$ where λ_1 is a repelling zeta fixed point; there appear to be at least three categories of such points: ψ_{-2n} (say) lying near the trivial zeros $-2n = -20, -22, ...$; zeta fixed points ψ_{ρ^*} near each nontrivial Riemann zero ρ^*, and eight fixed points lying at the boundary of the main cardioid (right panel, Figure 3.2.) How near? In the case of the ρ^*, one can form an impression by keeping in mind that this figure depicts a 120 by 120 square (section 8.) The distances $|-2n - \psi_{-2n}|$ are a great dealer smaller; we omit the details.

There are exactly two filaments F with degree $k_F = 1$ decorating the main cardioid; one of them contains ρ_N in its $|N|^{\text{th}}$ bulb $= \beta_N$, say. Our observations are consistent with the following proposition. The point ψ_{ρ_N} lies at the border of the $|N|^{\text{th}}$ bulb of a filament F^* with $k_{F^*} = 2$ decorating β_N. This ramifies: if ψ_{ρ_N} lies at the border of the $|N|^{\text{th}}$ bulb of a filament F^* then there is a child filament F' of F^* such that ψ_{ρ_N} lies at the border of the $|N|^{\text{th}}$ bulb of F' and $k_{F'} = k_{F^*} + 1$.

This is illustrated by the left column of Figure 5.1 for $N = 1, 2, 3, 4$. It depicts quadrant plots of $s \mapsto \zeta(s) - s$, so that ψ_{ρ_N} shows up as four-color junctions on the depicted filament (say, F_2.) The right column shows quadrant plots of $\zeta^{\circ3}, \zeta^{\circ4}, \zeta^{\circ5}, \zeta^{\circ6}$ in rows 1, 2, 3 and 4, respectively, all superposed on plots of A_ϕ. The squares have side length $.2, .02, .002$, and $.0002$ in rows 1, 2, 3 and 4, respectively. The center of the squares in row N is ψ_N, so the panels are depicting the region around this point at smaller and smaller scales.

Figure 4.1 displays the original indications we had that some branches of the inverse of zeta lie on spirals. It zooms in on the illustration of ψ_{ρ_1} in the left
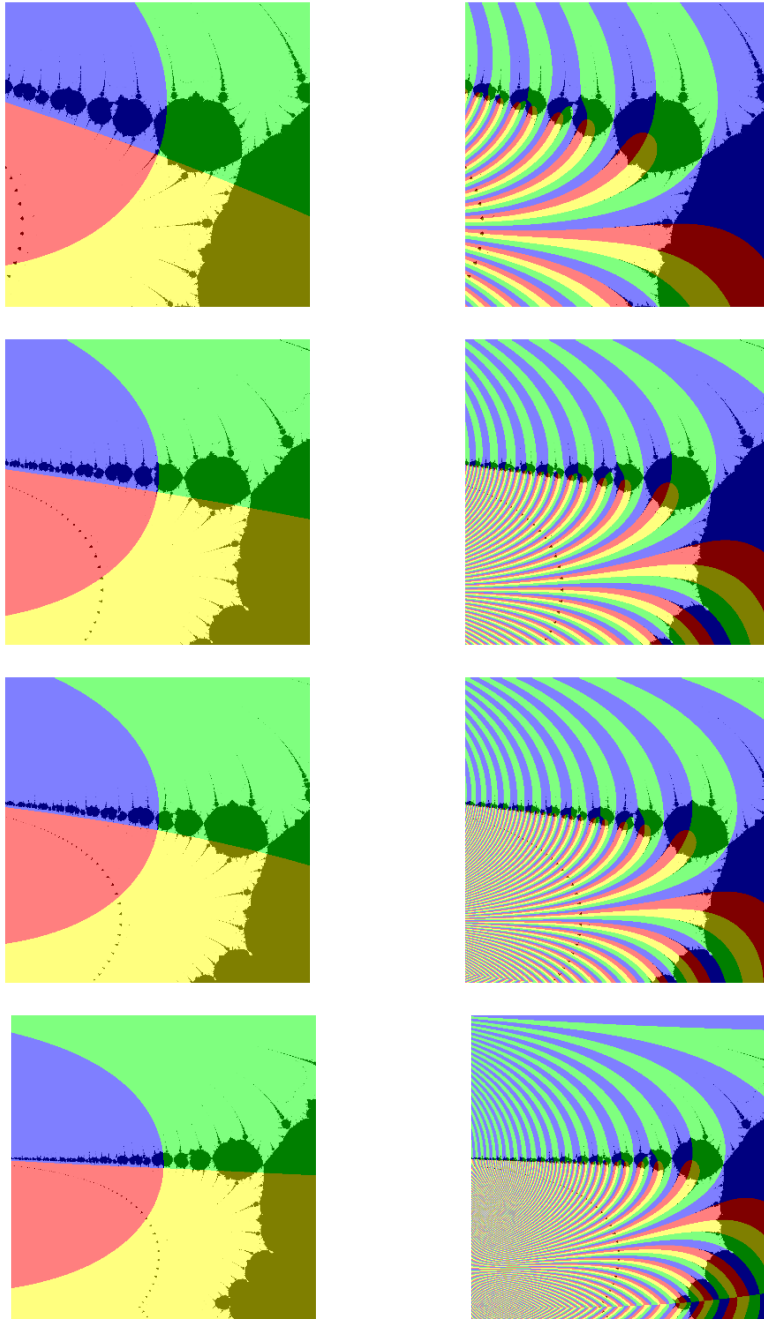
FIG. 5.1: TOP TO BOTTOM: $\psi_{\rho_n}, 1 \leq n \leq 4$; COLUMN 1: QUADRANT PLOTS OF $\zeta(s) - s$; COLUMN 2: QUADRANT PLOTS OF $\zeta^{\circ 2}$

19

panel of the top row of Figure 5.1. The center of that panel is the fixed point, lying on the border of a filament F_3 (say) decorating the lower border of the largest full bulb. In the right panel of the top row of Figure 4.1, a quadrant plot of $\zeta^{\circ 3}$ has been superimposed on a plot of the corresponding region of A_ϕ; we see that F_3 contains zeros of $\zeta^{\circ 3}$. (Simple tests show that they are nontrivial zeros in the sense of the introduction.) In the lower rows, the zoom is repeated and ψ_{ρ_1} is seen to lie near a still-smaller filament decorating the bulb near the center of the figure just above it. The right column depicts quadrant plots of $\zeta^{\circ 4}$, $\zeta^{\circ 5}$ and $\zeta^{\circ 6}$ for the squares opposite them in the left column. So in Figure 4.1 we are seeing zeros of these functions (again nontrivial.) They also appear (in virtue of the shapes of the underlying A_ϕ-bulbs) to be $\zeta^{\circ 3}, \zeta^{\circ 4}, \zeta^{\circ 5}$ pre-images of nontrivial Riemann zeros. The rapid reduction of scale from one row to the next attests to a similar reduction of the distances of these pre-images from ψ_{ρ_1} (which, as we have remarked, is not surprising.) The possibility that they may be traveling on spirals emerges from a look at the angles that the filaments F_3 and (say) F_4, F_5, F_6 make with the horizontal. These observations led us to do the numerical tests described in the last section.

We made a survey of the spirals $s_{\rho, \psi_{\rho^*}}$ for various choices of ρ and ρ^*. We made a table of $\psi_{\rho_n}, 1 \le n \le 100$ with 500 digits of precision and we used a table of nontrivial Riemann zeros with 300 digits of precision made by Andrew Odlyzko [9]. We made tables of the z_k in various $B_{\rho, \psi_{\rho^*}}$ to high precision, proceeding inductively. We set $z_1 = \rho$ and, given a value of z_k, after using *Mathematica's* FindRoot command to solve $\zeta(s) = z_k$ in the vicinity of ψ_{ρ^*}, we set z_{k+1} equal to the solution. We began with 300 z_k for each B and used tests of reliability of each z_k to truncate the list; typically, we ended up with a least 100 consecutive z_k.

We use polar coordinates $(r(z), \theta(z))$ to denote a typical point z on $s_{\rho, \psi_{\rho^*}}$ such that (1) $r(z) = |z - \psi_{\rho^*}|$, (2) $\theta(z)$ is chosen so that $\theta(z) \equiv \arg(z - \psi_{\rho^*})$ (mod 2π), and (3) $\theta(z)$ varies continuously and monotonically as z moves around the spiral in a fixed direction. In other words, $\theta(z)$ behaves up to a mutiplicative constant like a winding number. Then $r(z)$ appears to decay exponentially with $\theta(z)$. (Of course we are only able to check this for $z \in B_{\rho, \psi_{\rho^*}}$, that is, for the z_k we propose are interpolated by $s_{\rho, \psi_{\rho^*}}$, because no other test for membership in $s_{\rho, \psi_{\rho^*}}$ is available to us.) Therefore it was not practical to plot the spirals $s_{\rho, \psi_{\rho^*}}$ without re-scaling, so we plotted the points $(\log r(z), \theta(z))$ instead. This procedure everts the apparent spirals: if k, j are such that $r(z_k) < 1$ and $r(z_j) < 1$, then $r(z_j) < r(z_k)$ implies that the plotted point $(\log r(z_j), \theta(z_j))$ is further from the center of the re-scaled interpolating spiral than the point $(\log r(z_k), \theta(z_k))$: the reverse of the situation before re-scaling. (The direction of winding of the spiral is also reversed because the logarithms take negative values.) The points near the center of the re-scaled spiral depict z_k for smaller values of k for which z_k is closer to ρ and further from ρ^*. They are crowded so closely, in spite of our re-scaling, that the interpolating curve near ρ is obscured.

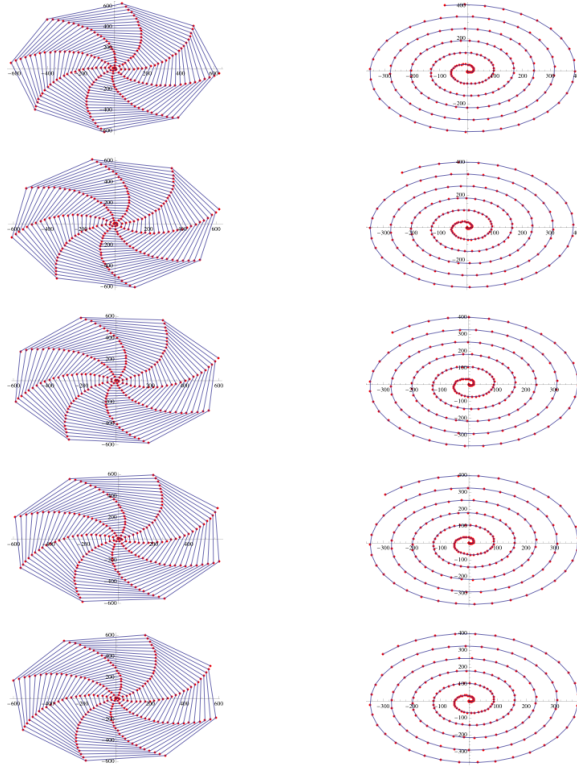Figure 5.2 depicts branches of backward orbits of $\rho_n(1 \leq n \leq 5)$ spiraling

FIG. 5.2: BACKWARD ORBIT BRANCHES FOR $\rho_n\,(1 \leq n \leq 5)$ CENTERED ON TWO CARDIOID ZETA FIXED POINTS

around two fixed point $\approx -14.613 + 3.101i$ (left column) and $\approx -5.28 + 8.803i$ (right column) on the border of the main cardioid; we omit the 500 digit decimal expansions, which are easy to compute using *Mathematica*'s FindRoot command. Figure 5.3 depicts branches of backward orbits of ρ_n spiraling around $\psi_{\rho_n}\,(1 \leq n \leq 10)$. (We omit their precise expansions for the same reason.)

5.2   An example: the case $\rho = \rho^* = \rho_1$.

The first panel of Figure 5.4 plots the point set $B_{\rho_1, \psi_{\rho_1}}$ (re-scaled as described, and shifted to place the apparent spiral's center at the origin.) It offers the appearance that the z_k (in red) form arms something like those of a spiral galaxy; this seems to be a result of nearly regular growth of $\theta(z_k)$ with k. But z_k for consecutive k do not lie in adjacent positions on these arms; in the second panel, the z_k are connected by chords in the same order as they appear in the sequence $B_{\rho_1, \psi_{\rho_1}}$: vertices v, w representing $z_v, w = \zeta(z_v)$ are connected by a
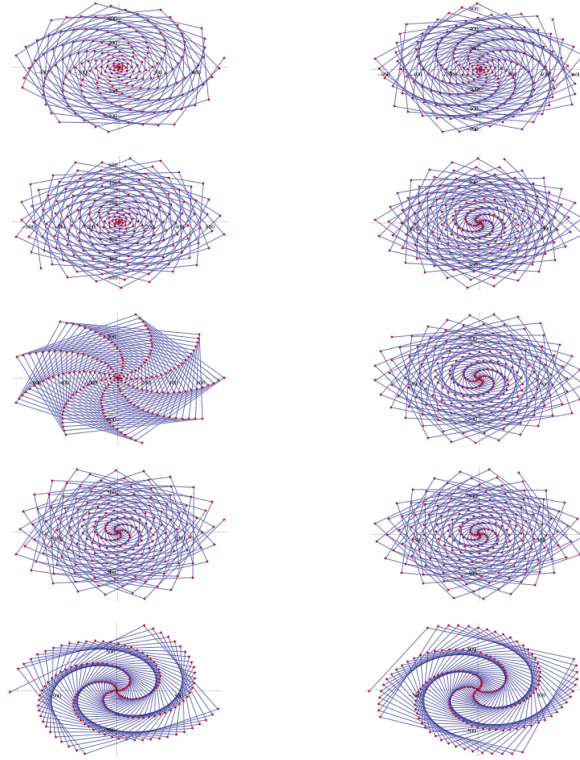
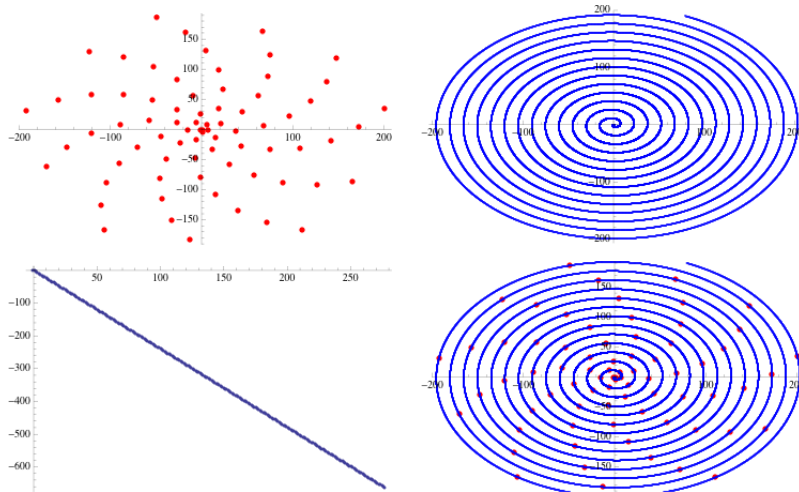FIG. 5.3: BACKWARD ORBIT BRANCHES FOR ρ_n NEAR $\psi_{\rho_n}, 1 \le n \le 10$

FIG. 5.4: LOGARITHMIC SCALING OF s_{ρ_1, ρ_1}

chord. The lower left panel of Figure 5.4 is a plot of $\log|z_k - \psi_{\rho_1}|$ vs. k; it is clear that the distances of the z_k (colored red) from the fixed point ψ_{ρ_1} at the center of the spiral are decaying exponentially. The lower right panel of Figure 5.4 depicts a spiral curve (colored blue) that approximately interpolates the z_k; we found this curve using the NonLinearModelFit command in *Mathematica*. The equation of the curve is

$$\log r(z) = a + b\theta(z) + c\exp(d\theta(z)),$$

with

$$a \approx 0.0557520330155195656039945957916152935\,3,$$

$$b \approx -2.39481894384498740085074310912697832305,$$

$$c \approx -2.868035591772194163533139948518488\,4 \times 10^{-120},$$

and

$$d \approx 0.97375124237020440301256901292961731822.$$

The absolute value of c is so small that this is quite close to being the equation of a logarithmic spiral. In the section on error terms below we will compare directly the loci of the z_k with logarithmic spirals.

In Figure 5.5, we study the variation in $\theta(z_k)$. The left panel plots $\delta_k = \theta(z_{k+1}) - \theta(z_k)$ against k and shows that the $\theta(z_k)$ are very nearly periodic in k. The right panel, which plots $\log|\delta_{k+1} - \delta_k|$ against k, shows that the de-
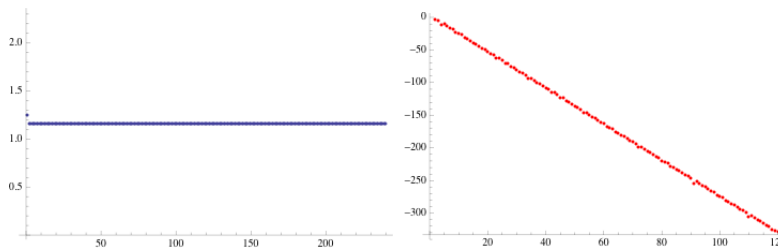

FIG. 5.5: LEFT: δ_k VS. k RIGHT: $\log|\delta_{k+1} - \delta_k|$ VS. k.

parture from periodicity in $\theta(z_k)$ actually appears to decay exponentially with k. However for other choices of ρ and ρ^* this no longer holds, and so it is an open question whether or not it would hold even in this example for very large k, that is, very close to the center of the spiral. We remark that the z_k could, of course, be distributed along a nearly-logarithmic spiral while also being distributed in a completely irregular or at least non-periodic way in the theta aspect, so the two questions are at least superficially independent.

Now suppose (r_1, θ_1) and (r_2, θ_2) lie on a true logarithmic spiral $\log r = a + b\theta$. The constants a, b are determined by any two points of the spiral, hence, if two pairs of points determine different values of a and b, then the curve that the

three (or four) points comprising the pairs lie on is not a logarithmic spiral. We used this idea to test $B_{\rho_1,\psi_{\rho_1}} = \{z_1, z_2, z_3, ...\}$ for the property of being interpolated by a logarithmic spiral. We performed the test by solving for a and b using the pairs $(z_1, z_k), k = 2, 3, ...$ In Figure 5.6 we have plotted the resulting
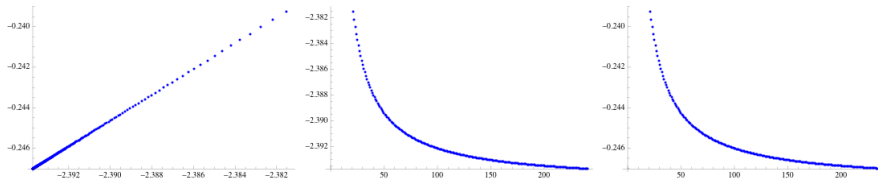

FIG. 5.6: PARAMETERS a, b FOR LOGARITHMIC CURVE $\log r = a + b\theta$ INDUCED BY SUCCESSIVE POINTS OF B_{ρ_1,ρ_1}. LEFT: a VS. b; CENTER: b VS. k; RIGHT: a VS. k

values of a against b, b against k, and a against k. Evidently a is roughly linear in b, and both a and b appear to converge as k grows without bound. Thus the interpolating curve is not a logarithmic spiral, for then a and b would be constants. But the convergence of a and b suggests that the interpolating spiral $s_{\rho_1,\psi_{\rho_1}}$ resembles a logarithmic spiral more and more closely as it winds inward towards ψ_{ρ_1}.

5.3 Backward orbits near the trivial zeros.

There appear to be real zeta fixed points ψ_{-2n} near each trivial zero $-2n \leq -20$. Whether they lie slightly to the right or to the left of $-2n$ along the real axis appears to depend upon the parity of n. This reflects the alternating left-right orientations of copies (zeta pre-images) of the basin of attraction A_ϕ we see in Figure 3.4.

A branch $B_{\rho,\psi_{-2n}}$ of the backward orbit of each nontrivial Riemann zero ρ lies on a curve appearing to pass through or terminate at ψ_{-2n}: if $-2n \equiv 0$ (mod 4), then the curve appears to terminate at ψ_{-2n}. These curves closely resemble straight line segments. Error terms are discussed in section 6. If $-2n \equiv 2$ (mod 4), then (supposing, for the moment, that the curve really is a line segment) ψ_{-2n} lies near its midpoint. In Figure 5.7, several of the backward orbits are depicted, re-scaled logarithmically as above.

This observation is consistent with the hypothesis that $B_{\rho,\psi_{-2n}}$ is interpolated by a spiral such that the $a_k \in B_{\rho,\psi_{-2n}}$ satisfy $|\arg(a_k - \psi_{-2n}) - \arg(a_{k+1} - \psi_{-2n})| \approx 2\pi$ for all k if $-2n \equiv 0$ (mod 4), or $|\arg(a_k - \psi_{-2n}) - \arg(a_{k+1} - \psi_{-2n})| \approx \pi$ if $-2n \equiv 2$ (mod 4). We discuss this further in sections 5.5 and 6.2.
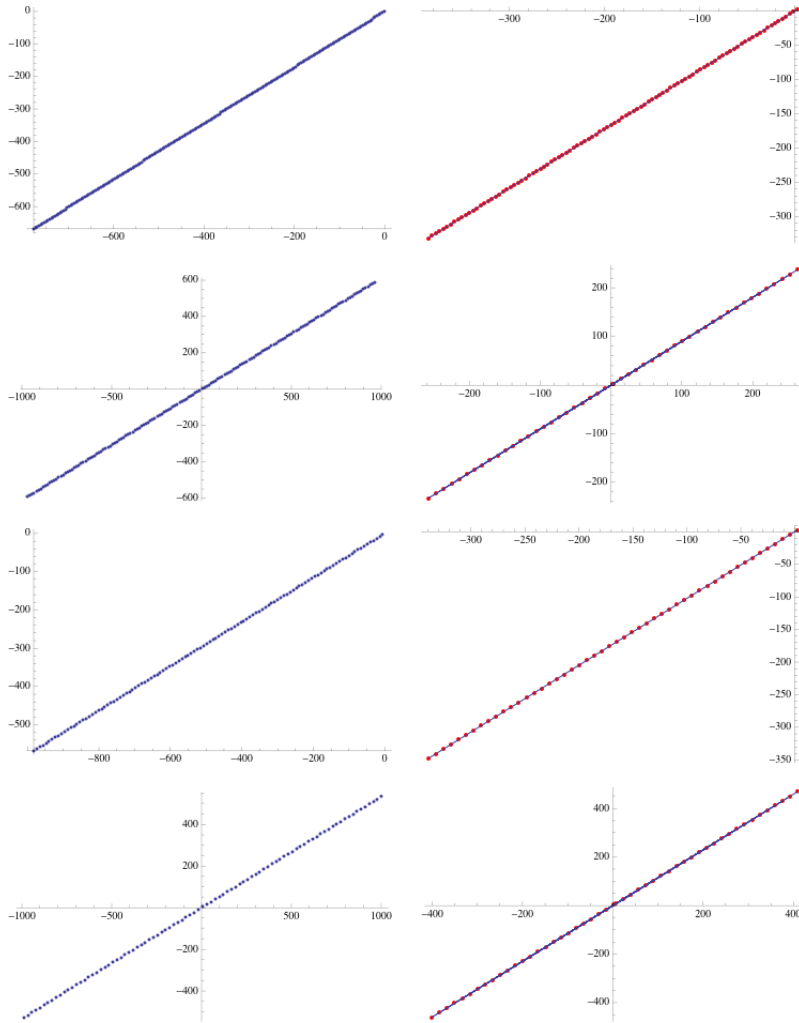
FIG. 5.7: COLUMN 1: BACKWARD ORBITS OF ρ_1 NEAR $\psi_{-2n}, 10 \leq n \leq 13$
COLUMN 2: BACKWARD ORBITS OF ρ_{n-9} NEAR $\psi_{-2n}, 10 \leq n \leq 13$
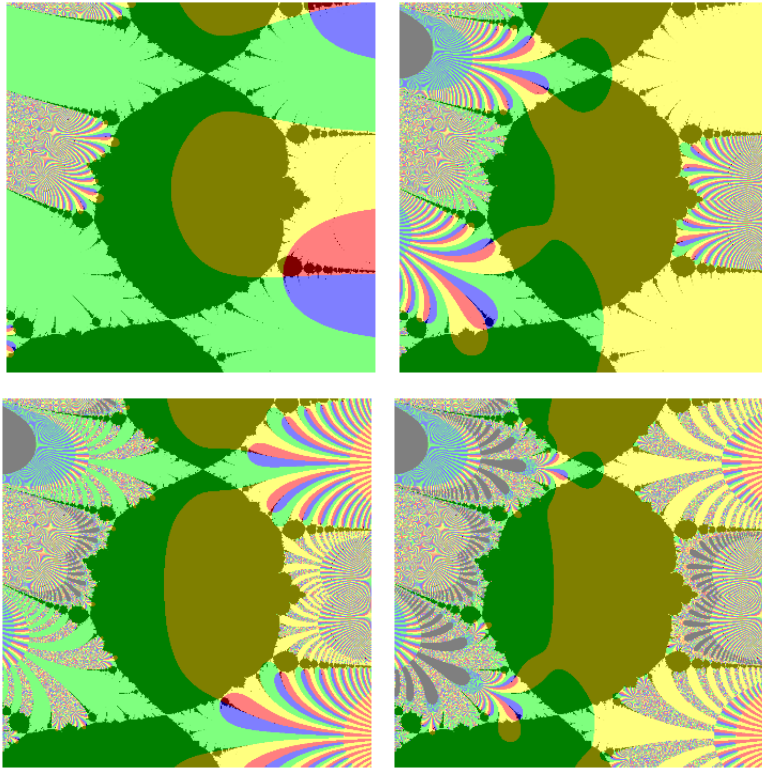
FIG. 5.8: QUADRANT PLOTS OF $s \mapsto \zeta^{\circ n}(s) - s$, $2 \leq n \leq 5$, NEAR THE BULB AROUND ρ_1

5.4 Several spirals that together interpolate a branch.

Figure 5.8 depicts members of zeta n-cycles (zeros of $s \mapsto \zeta^{\circ n}(s) - s$) near the bulb of A_ϕ containing ρ_1 for $2 \leq n \leq 5$. As n increases the pattern of distribution of these zeros becomes more and more obscure. The situation near ρ_1 appears to be typical of that near all nontrivial zeros of zeta iterates.

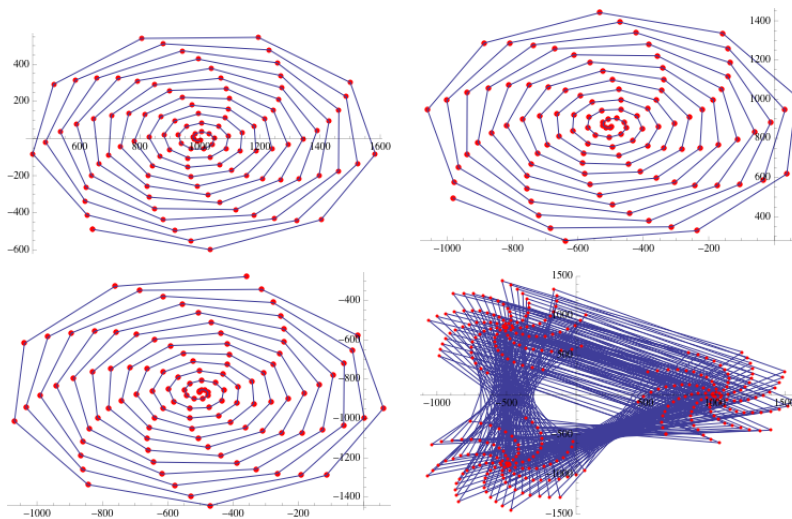Figure 5.9 illustrates the branch $B_{\rho_1, \Lambda}$ of the backward orbit of $\zeta^{\circ -}(\rho_1)$ induced

FIG. 5.9: THE BRANCH OF A ρ_1 BACKWARD ORBIT INDUCED BY A ZETA 3-CYCLE

by a 3-cycle $\Lambda = (\lambda_1, \lambda_2, \lambda_3)$ with $\lambda_1 \approx 3.95896 + 24.2362i$. The red vertices of a given chord of the graph represent points in the branch. Geometrically, Figure 5.9 is doubly abstract: (1) The spirals have been positioned so that their centers are placed at $1000 + 0i, 1000(\cos(\frac{2\pi}{3}) + i\sin(\frac{2\pi}{3}))$ and $1000(\cos(\frac{4\pi}{3}) + i\sin(\frac{4\pi}{3}))$ for the sake of legibility; and (2) the spirals are everted: they have been re-scaled logarithmically, so that points closer to the center appear, in the figure, to be farther from the center. The row 2, column 2 panel shows vertices representing elements of $B_{\rho_1, \Lambda}$ and edges between vertex pairs $(v, \zeta(v))$, while the other panels depict the spirals separately; these are portraits of $b_j (j = 1, 2, 3)$. In these three figures, each vertex pair $(v, \zeta^{\circ 3}(v))$ is connected by an edge.

5.5 Angular distribution of branches along the spirals.

A structural invariant, which seems to determine the number of arms visible in our plots of branches of $f^{\circ -}(z)$, is the function $\delta_{f,z,\psi} : k \mapsto \arg(a_k - \psi) - \arg(a_{k+1} - \psi)$, where the a_k's are members of a particular branch of $f^{\circ -}(z)$ converging to ψ.

The values of δ_k in the case discussed in section 5.2 correspond in the present notation to those of $\delta_{\zeta,\rho_1,\psi_1}(k)$. They appear to change very slowly with k, and this behavior seems to be what gives rise to the appearance of discrete arms in plots of branches of $\zeta^{\circ-}(\rho_n)$.

Among the zeta fixed points very near trivial zeros, the only values of $\delta_{\zeta,\rho_n,\psi_{-2n-18}}(k)$ that we see (Figure 5.7) are $\approx \pi$ and $\approx 2\pi$, distributed, as we have noted above, according to the mod 4 residue classes of the zeros.

Because $\delta_{\zeta,\rho_n,\psi_{\rho_n}}(k)$ apparently converges rapidly as $k \to \infty$ (as in Figure 5.5 where $n = 1$), we take the value of $\delta_{\zeta,\rho_n,\psi_{\rho_n}}(100)$ as a proxy for $\lim_{k\to\infty} \delta_{\zeta,\rho_n,\psi_{\rho_n}}(k)$. Then our calculations are consistent with the proposition
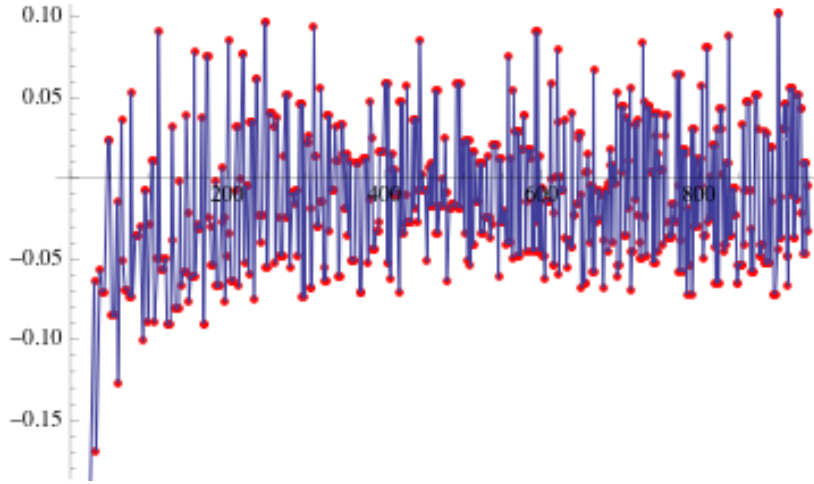

FIG. 5.10:

$$\frac{\delta_{\zeta,\rho_n,\psi_{\rho_n}}(100) - \pi/2}{\pi/2}, 1 \le n \le 600$$

that $\lim_{k\to\infty} \delta_{\zeta,\rho_n,\psi_{\rho_n}} \approx \pi/2$ (Figure 5.10.) Very small differences in this limit as n varies appear to determine very different shapes for the discrete arms visible in our plots.

We have observed in all of our experiments that the visible structure of a branch of $f^{\circ-}(z)$ depends upon the fixed point at its center and not on z, so $\delta_{f,z,\psi}$ should depend only upon f and ψ. Contrary to the impression suggested by our notation, it should be independent of z, but we cannot exclude the possibility that there are counterexamples to this idea.

28

5.6 Logarithmic models of spirals interpolating branches of the backward orbit of zeta.

The branches $B_{\rho,\psi} = (a_0 = \rho, a_1, a_2, ...)$ of $\zeta^{\circ-}(\rho)$ for nontrivial Riemann zeros ρ converging to zeta fixed points ψ are interpolated by curves that resemble logarithmic spirals. We carried out experiments in which we looked for approximations of these interpolating curves by such spirals. We chose branches of the argument function, varying with k and evaluated at $a_k - \psi$, such that an angle θ_k was assigned to $a_k - \psi$ which was the least such angle $> c + \max_{j<k} \theta_j$ for $c = 0$ or 1. The angle θ_0 was the value of $\arg(a_0 - \psi)$ from the branch of argument chosen automatically by *Mathematica*. The choice of c was dictated by requiring that θ_k act like a winding number about ψ evaluated at the points a_k. For ψ near a trivial zero, $c = 1$ was chosen; for ψ near a nontrivial zero, $c = 0$.

For $r_k = |a_k - \psi|$ plots of the sets of pairs $(\theta_k, \log r_k), k \geq 0$, appear to lie on curves resembling straight lines. For spirals centered at zeta fixed points ψ_{ρ_n} near the ρ_n, we approximated these lines using *Mathematica*'s FindFit command. Figure 5.11 is a pair of plots of m_n and b_n against n for models
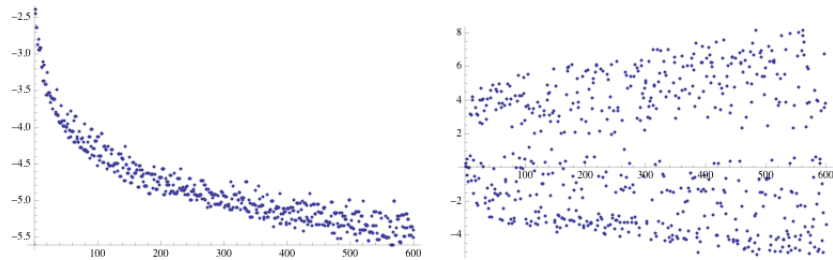

FIG. 5.11: SLOPES m_n (LEFT PANEL) AND INTERCEPTS b_n (RIGHT PANEL) IN LOG-LINEAR MODELS $\widetilde{r} = \exp(m_n\theta + b_n)$ OF SPIRALS INTERPOLATING BRANCHES OF ρ_n CENTERED AT ψ_{ρ_n} WITH $r = |z - \psi_{\rho_n}|$ AND $\theta = \arg(z - \psi_{\rho_n})$

$|z - \psi_{\rho_n}| = \exp(m_n\theta + b_n)$ fitted to branches of $\zeta^{\circ-}(\rho_n), 1 \leq n \leq 600$. In particular, we write $\widetilde{r_k} = \exp(m_n\theta_k + b_n)$ for our estimate of r_k. These seem to be first-order approximations to genuine interpolating curves; the error-term will be discussed in the next section.

Investigating spirals centered at the zeta fixed points ψ_{2n} that lie near the trivial zeros was carried out in a different way. We were able to collect a substantial amount of data (meaning for the first 200 members of the branches) for the $\psi_{\rho_n}, n \leq 600$ using 500-digit precision. On the other hand, even with 1000-digit precision, we were able to collect data only on the first twenty elements of branches centered at the ψ_{-2n} for $n \leq 30$ before the use of the FindFit command to get a linear model for the pairs $(\theta_k, \log r_k)$ produced error messages from *Mathematica*.

Fortunately, the branches spiraling about the ψ_{-2n} appear to be better behaved than the ones spiraling about the ψ_{ρ_n}. For each pair (n, n^*) the branch $B_{\rho_n, \psi_{-2n^*}}$ is apparently interpolated both by a curve very nearly a logarithmic spiral and by another curve which is very nearly a straight line passing through the points ρ_n and ψ_{-2n^*}. As we will see in the next section, the fit of the branches to the straight line passing through these two points is so good that we use it as our second model, together with the assumption that the $\theta_k = a\pi k +$ (a constant depending only on n and n^*), with $a = 1$ or 2 depending as we have explained only on the parity of n^*. It was feasible to find linear models for the maps $k \mapsto \log r_k$. Combining the assumptions about the θ_k with the linear models we construct for the $\log r_k$ gives logarithmic models for the interpolating spirals. We test these models in the next section.

We chose to examine the behavior of branches $B_{\rho_n, \psi_{-2n-18}}$ of $\zeta^{\circ-}(\rho_n)$ because, among zeta fixed points close to the trivial zeros $-2n$, the greatest one (the one that lies rightmost along the real axis) is very close to -20. Figure 5.12 is a plot
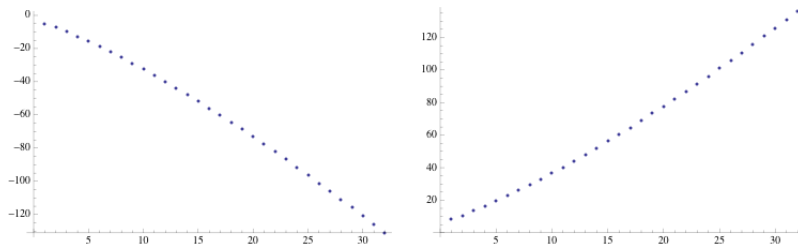

FIG. 5.12: SLOPES m_n (LEFT PANEL) AND INTERCEPTS b_n (RIGHT PANEL) IN MODELS $\widehat{r_k} = \exp(m_n k + b_n)$ OF SPIRALS INTERPOLATING BRANCHES OF ρ_n CENTERED AT ψ_{-2n-18}

corresponding to Figure 5.11 for the zeta fixed points ψ_{-2n-18}. Here we have $B_{\rho_n, \psi_{-2n-18}} = (a_0 = \rho_n, a_1, a_2, ...)$. Writing $r_k = |\psi_{-2n-18} - a_k|$, we took m_n and b_n to be, respectively, the means of the slopes and intercepts of the chords connecting consecutive pairs $p_k = (k, \log |a_k - \psi_{-2n-18}|)$. Thus our model for $r_k = |a_k - \psi_{-2n-18}|$ is $\widehat{r_k} = \exp(m_n k + b_n)$. We discuss it further this in the following section.

6 ERROR TERMS

We will take the phrase "error term" to encompass complex-valued deviations from a given estimate as well as their absolute values. Like the original estimates, the curves followed by complex-valued deviations appear to have the form of logarithmic spirals. This raises the prospect of an infinite regress, which might perhaps lead to an exact expression for the best interpolating curves, but we have postponed any investigation of this idea.

6.1 Deviation of backward orbits from logarithmic spirals.

6.1.1 Branches converging to fixed points near non-trivial zeros.

(This subsection provides some of our evidence for Conjecture 1.) For various Riemann zeros ρ and zeta fixed points ψ, we plotted the relative complex-valued deviations $d(n,k) :=$

$$\left| \frac{(a_k - \psi) - \widetilde{r_k} e^{i\theta_k}}{a_k - \psi} \right|$$

of the members of $B_{\rho,\psi}$ from the logarithmic spirals best approximating the curves interpolating $B_{\rho,\psi}$. (Here, "best" means that we used *Mathematica*'s FindFit command to fit the points $(\theta(a_k), \log|a_k - \psi|)$ to straight lines.) The
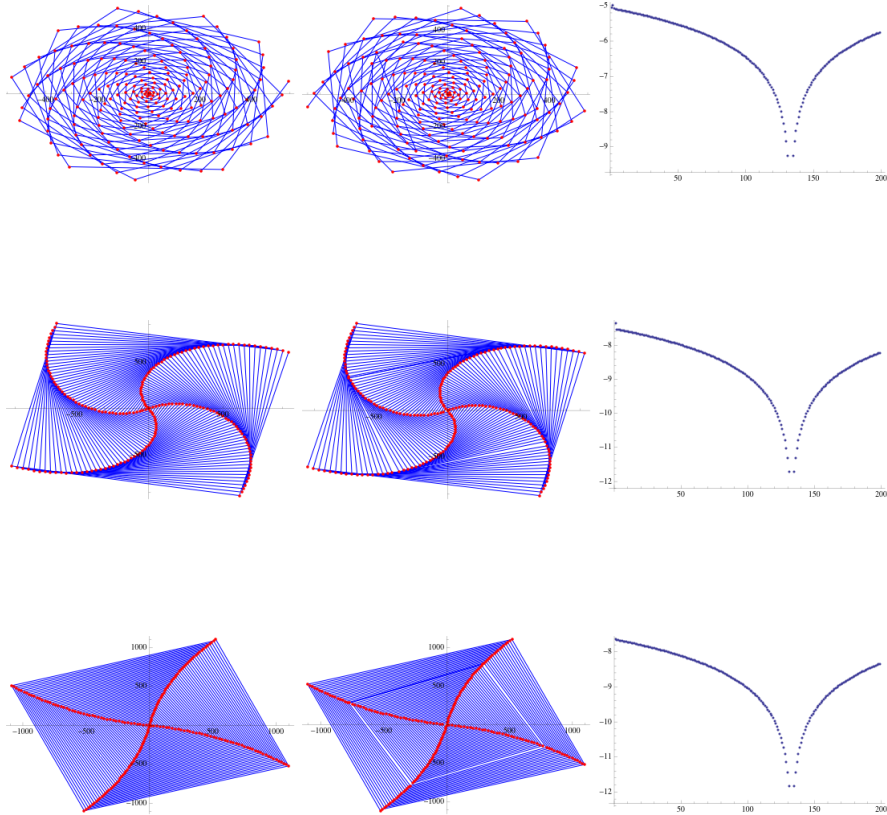

FIG. 6.1: $B_{\rho_n, \psi_n}, n = 1, 28, 48$: COLUMN 1: ORIGINAL BRANCHES; COLUMN 2: DEVIATIONS OF B_{ρ_n, ψ_n} FROM LOGARITHMIC SPIRALS; COLUMN 3: $\log d(n, k)$ VS. k

runs depicted in Figure 6.1 portray both kinds of plots for $\rho = \rho_n, \psi = \psi_{\rho_n}$

31

for $n = 1, 28$, and 48. It seems noteworthy that the two kinds of plots resemble each other so closely, but inspection demonstrates that they are not identical.

The values of $\log d(n, k)$ for $n = 1, 28$, and 48 are also plotted in Figure 6.1 (column 3.) The magnitude of the $d(n, k)$ appears to decay exponentially for $k <$ roughly 130; for larger k, however, the magnitude of the deviations appears to grow exponentially without exceeding e^{-6} for $k \leq 200$. We think that the shape of this curve, which is typical, is an artificial effect of the FindFit command on a file of 200 pieces of data: the fit is best near the center of the data file.

For a fixed point $\psi = \psi_{\rho_n}$ near a nontrivial zero $\rho = \rho_n$, we used the initial 200 elements of each branch $B_{\rho,\psi}$ as a proxy for $B_{\rho,\psi}$ to study the relative deviations of the curve interpolating it from a logarithmic spiral. Taking $\beta = 200$ for the moment, let us set

$max_{n,\beta} := \max_{1 \leq k \leq \beta} d(n, k),$

$max^*_{n,\beta} := \sqrt{n/\log n} \times x_{n,\beta},$

let $mean_{n,\beta}$ denote the mean of $d(n, 1), d(n, 2), ..., d(n, \beta)$, and let

$mean^*_{n,\beta} := \sqrt{n/\log n} \times mean_{n,\beta}.$

The panel in row 1 column 1 of Figure 6.2 is a plot of 600 values of $mean^*_{n,\beta}$.
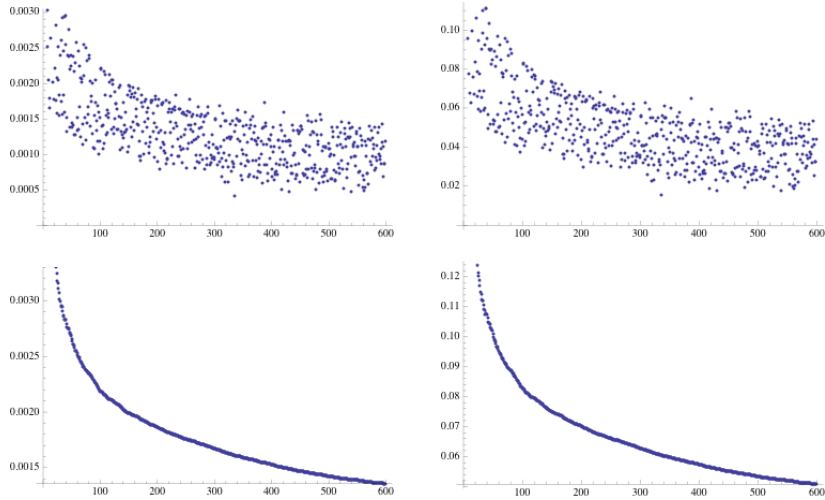

FIG. 6.2: $mean^*_{n,\beta}$ (LEFT) AND $max^*_{n,\beta}$ (RIGHT); $\beta = 200, 1 \leq n \leq 600$

The panel in row 1 column 2 is a plot of $max^*_{n,\beta}$. The plots in row 2 are smoothings of the plots in row 1: for each n, they depict means of $mean^*_{j,\beta}$ and $max^*_{j,\beta}$

32

over the range $1 \leq j \leq n$.

These plots are consistent with the proposition that, for $\beta = 200$, $mean_{n,\beta}$ and $max_{n,\beta}$ both $= O\left(\sqrt{\frac{\log n}{n}}\right)$ with both implied constants < 1. More optimistically, perhaps, the plots are consistent with the hypothesis that $mean_{n,\beta}$ and $max_{n,\beta}$ both $= o\left(\sqrt{\frac{\log n}{n}}\right)$.

We tested the same idea after replacing $\sqrt{\frac{\log n}{n}}$ with powers $\left(\frac{\log n}{n}\right)^{\epsilon}$ for $\frac{1}{2} < \epsilon < 1$. It seems possible that the supremum of ϵ for which these statements might be true lies in the half-open interval $[.8, .9)$. It also seems possible that this supremum is a decreasing function of n. We omit the relevant plots.

6.1.2 Branches converging to fixed points near the trivial zeros.

(This subsection provides some of our evidence for Conjecture 2.) Let the branch $B_{\rho_n,\psi_{-2n-18}}$ of $\zeta^{\circ-}(\rho_n) = (a_0 = \rho_n, a_1, a_2, ...)$. Before we test a logarithmic model for the decay of $r_k = |a_k - \psi_{-2n-18}|$, we want to assess how well $B_{\rho_n,\psi_{-2n-18}}$ fits the straight line passing through ρ_n and ψ_{-2n-18}. We measured the vertical deviation of the $a_k \in B_{\rho_n,\psi_{-2n-18}}$ from the straight line passing through both ρ_n and ψ_{-2n-18} as a fraction of the heights of the a_k. We make the following definitions:

M_n and B_n are the slope and intercept respectively of the straight line passing through ρ_n and ψ_{-2n-18}

and

$$d^{trivial}(n,k) :=$$
$$\left| \frac{\Im(a_k) - (M_n\Re(a_k) + B_n)}{\Im(a_k)} \right|,$$

$mean_{n,\beta}^{trivial} = $ the mean of the $d^{trivial}(n,k), 1 \leq k \leq \beta,$

and

$max_{n,\beta}^{trivial} = \max_{1 \leq k \leq \beta} d^{trivial}(n,k).$

The left panel of Figure 6.3 is a plot of $\log mean_{n,\beta}^{trivial}, 1 \leq n \leq 32$ and $\beta = 20$. The right panel is a corresponding of $\log max_{n,\beta}^{trivial}$. Evidently, the a_k lie near the specified lines, and agreement with the lines improves rapidly as n increases.

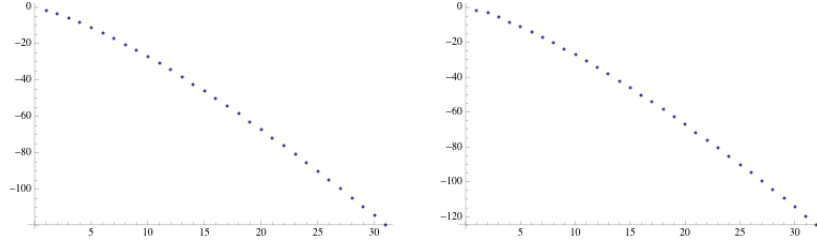Next we define for $a_k \in B_{\rho_n,\psi_{-2n-18}}$

FIG. 6.3: $\log mean_{n,\beta}^{trivial}$ (LEFT) AND $\log max_{n,\beta}^{trivial}$ (RIGHT);
$\beta = 20, 1 \le n \le 32$

$$r_{n,k} = |a_k - \psi_{-2n-18}|,$$

for $k > 1, m_{n,k} =$ the slope of the chord connecting the ordered pairs $(k, \log r_{n,k})$ and $(k, \log r_{n,k-1})$ in $\mathbf{R}^2$,

$$m_{n,\beta} = \text{mean of the } m_{n,k}, 1 \le k \le \beta,$$

and we define a y-intercept function $b_{n,\beta}$ analogously. The error functions are defined as follows:

$$d^{model}(n, k, \beta) := \left| \frac{\log r_{n,k} - (m_{n,\beta}k + b_{n,\beta})}{\log r_{n,k}} \right|,$$

$$mean_{n,\beta}^{model} = \text{the mean of the } d^{model}(n, k, \beta), 1 \le k \le \beta,$$

and

$$max_{n,\beta}^{model} = \max_{1 \le k \le \beta} d^{model}(n, k, \beta).$$

The left panel of Figure 6.4 is a plot of $\log mean_{n,\beta}^{model}, 1 \le n \le 32$ and $\beta = 20$.

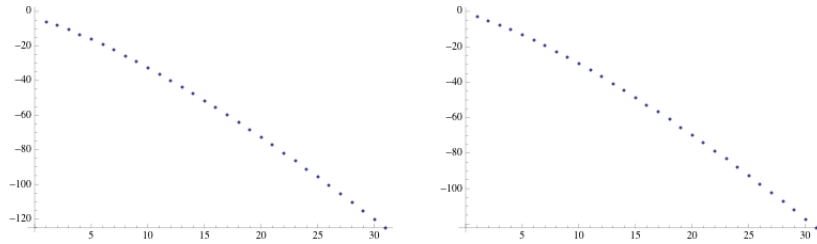FIG. 6.4: $\log mean_{n,\beta}^{model}$ (LEFT) AND $\log max_{n,\beta}^{model}$ (RIGHT);
$\beta = 20, 1 \le n \le 32$

The right panel is a corresponding of $\log max_{n,\beta}^{model}$. Once more the fit is good and improves rapidly as n increases.

34

7 An analogy from fluid mechanics.

It did not seem plausible to us that something special about Riemann zeros ρ should force the branches $\zeta^{\circ-}(z), z = \rho$ in particular, to be attracted to repelling fixed points ψ along logarithmic spirals. As we remarked in the introduction, dynamical systems theory leads one to expect that the ψ should attract all of the nearby branches $\zeta^{\circ-}(z)$ whether or not $\zeta(z) = 0$, and (one speculated) probably along roughly similar curves. Logarithmic spirals appear in fluid mechanics (see, *e.g.*, [8], v.2, pp. 186-188 or [10], p. 358.) By analogy with the streamlines of a vortex in a fluid, we speculated that the existence of spiral curves connecting zeros of zeta to repelling zeta fixed points might be a consequence of a scenario in which there is an infinite family of such spirals related by rotations around the fixed point. By this we mean a family of spirals s parameterized by real numbers x, varying continuously with x in a sense made explicit by condition (1) below, such that if s_x and $s_{x+\theta}$ are two such spirals with common center a zeta fixed point ψ, then

(1) $s_{x+\theta} - \psi = e^{i\theta}(s_x - \psi)$

(condition (1) being an equation of homotheties) and

(2) $z \in s_x \Rightarrow$ (i) $\zeta(z) \in s_x$ and (ii) there exists a branch $B_z \subset s_x$ of $\zeta^{\circ-}(z)$ such that $\lim B_z = \psi$.

In this scenario, the spiral curves would be congruent in the sense of Euclidean geometry and exactly one spiral would intersect the critical line at each ρ_n without appealing to special properties of the zeros. We have verified the existence of spiral branches B_z of $\zeta^{\circ-}(z)$ for various z on the critical line other than Riemann zeros without meeting a counterexample. Like the spirals we have already described, they are approximately logarithmic; we omit the relevant plots.

Condition (1) imposes rotational invariance on the s_x. This suggests the possibility that the branches of $\zeta^{\circ-}$ interpolated by them enjoy the same property. Suppose u and $\zeta(u)$ lie on s_x with center ψ and let $R_{\theta,\psi}(z) := e^{i\theta}(z - \psi) + \psi$ be the function that takes z to its image under rotation by an angle θ around ψ. Under perfect rotational invariance, not only of the spirals s_x but of the branches of $\zeta^{\circ-}(z)$ for particular z that they interpolate, the numbers $R_{\theta,\psi}(\zeta(u)) - \zeta(R_{\theta,\psi}(u))$ must vanish. Therefore we studied the $R_{\theta,\psi}(\zeta(u)) - \zeta(R_{\theta,\psi}(u))$. We restricted ourselves to $u \in \zeta^{\circ-}(z)$ for various z, not only because these are the main objects of interest, but because our only reliable information about the spirals comes from their interpolation of the branches $B_\psi = (a_0, a_1, a_2, ...)$ of $\zeta^{\circ-}(z)$, and so our only useful candidates for points in s are the members of such branches.

Logarithmically scaled plots (which we omit) of the discrepancies (say) $R_{\theta,\psi}(\zeta(a_n)) - \zeta(R_{\theta,\psi}(a_n))$ indicate that these numbers decay in modulus exponentially and

rotate around the origin in a nearly linear fashion with n. In other words, they themselves describe curves that are approximated by logarithmic spirals.

8 APPENDIX: THE FIGURES

8.1 Figure 1.1

Figure 1.1 a 120 by 120 square with center $1 + 0i$.

8.2 Figure 2.1

Figure 2.1 depicts a 6 by 6 square with center zero.

8.3 Figure 3.1

Figure 3.1 shows an 8 by 8 square with center $-5 + 9.5i$.

8.4 Figure 3.2

Figure 3.2 shows a 120 by 120 square with center zero.

8.5 Figure 3.3

Figure 3.3 depicts a 60 by 60 square with center zero.

8.6 Figure 3.4

The upper left panel of Figure 3.4 shows a 2.4×10^{-5} by 2.4×10^{-4} square centered at -28. The upper right panel shows a 2.4×10^{-4} by 2.4×10^{-4} square centered at -26. The lower left panel shows a .004 by .004 square centered at -24. The lower right depicts a .07 by .07 square centered at -22.

8.7 Figure 3.5

The panel in row 1 column 1 of Figure 3.5 depicts a 10 by 10 square centered at ρ_1. The other panels show a square with side length .006 and center $\rho_1 + 4.1215 - .4015i \approx 4.6215 + 13.7332i$.

8.8 Figure 3.6

Each panel of Figure 3.6 is a 30 by 30 square with center $= -5$.

8.9 Figure 4.1

The squares depicted in Figure 4.1 have side length .2, .02, .002, and .0002 in rows 1, 2, 3 and 4, respectively. The center of each square is $\psi_{\rho_1} \approx -2.3859 + 16.271i$.

8.10 Figure 5.1

All the panels of Figure 5.1 depict A_ϕ in 2 by 2 squares. In rows 1 - 4, the centers are ψ_{ρ_1} - ψ_{ρ_4}, respectively, where $\psi_{\rho_2} \approx -2.0369 + 21.9931i$, $\psi_{\rho_3} \approx -1.6935 + 26.5283i$, and $\psi_{\rho_4} \approx -1.7496 + 30.8158i$.

8.11 Figure 5.2

In Figure 5.2, column 1 depicts branches of $\zeta^{\circ-}(\rho_n)$, $1 \le n \le 5$, centered at a zeta fixed point $\approx -14.613 + 3.108i$; column 2 depicts branches of $\zeta^{\circ-}(\rho_n)$, $1 \le n \le 5$, centered at a zeta fixed point $\approx -5.279 + 8.803i$.

8.12 Figure 5.3

In Figure 5.3 (referring to the caption), the value of n in row a, column b is $n = 2a + b - 2$.

8.13 Figure 5.8

Figure 5.8 depicts four views of a 12 by 12 square with center ρ_1.

8.14 Figure 5.9

Figure 5.9 depicts the branch $B_{\rho_1, \Lambda}$ of the backward orbit of $\zeta^{\circ-}(\rho_1)$ induced by a 3-cycle $\Lambda = (\lambda_1, \lambda_2, \lambda_3)$ with $\lambda_1 \approx 3.95896 + 24.2362i$.

References

[1] Broughan A, Kevin, and A. Barnett. The holomorphic flow of the riemann zeta function. *Mathematics of computation*, 73(246):987–1004, 2004.

[2] B. Cloitre. Personal communication.

[3] J. Arias de Reyna. X-ray of riemann zeta-function, 2003. arXiv:math/0309433.

[4] Xin-Hou Hua and Chung-Chun Yang. *Dynamics of Transcendental Functions*. Gordon and Breach Science Publishers, Australia Canada China France Germany India Japan Luxembourg Malaysia The Netherlands Russia Singapore Switzerland, 1998.

[5] T. Kawahira. Riemann's zeta function, newton's method, and holomorphic index, poster presented at kansuron's summer seminar, 1998.

[6] C. King. A dynamical key to the riemann hypothesis, 2011. arXiv:1105.2103.

[7] C. King. Fractal geography of riemann zeta and related functions, 2011. http://www.dhushara.com/Dark Heart/geozeta/geo.pdf.

[8] A. I. Markushevich. *Theory of Functions of a Complex Variable*. Chelsea Publishing Company, New York, N. Y, 1977. revised English Edition Translated and Edited by R.A. Silverman.

[9] A. Odlyzko. Tables of zeros of the riemann zeta function. www.dtc.umn.edu/odlyzko/zeta_tables/index.html.

[10] J. H. Spurk and N. Aksel. *Fluid Mechanics, Second Edition*. Springer-Verlag, Berlin Heidelberg, 2008, 1997.

[11] S. C. Woon. Fractals of the julia and mandelbrot sets of the riemann zeta function, 1998. arXiv:chao-dyn/9812031.

barrybrent@member.ams.org